Universiteit Utrecht

Master Thesis

Thermal Magnon Hall Effect in FM/AFM Skyrmionic Structures

Ilias Samathrakis

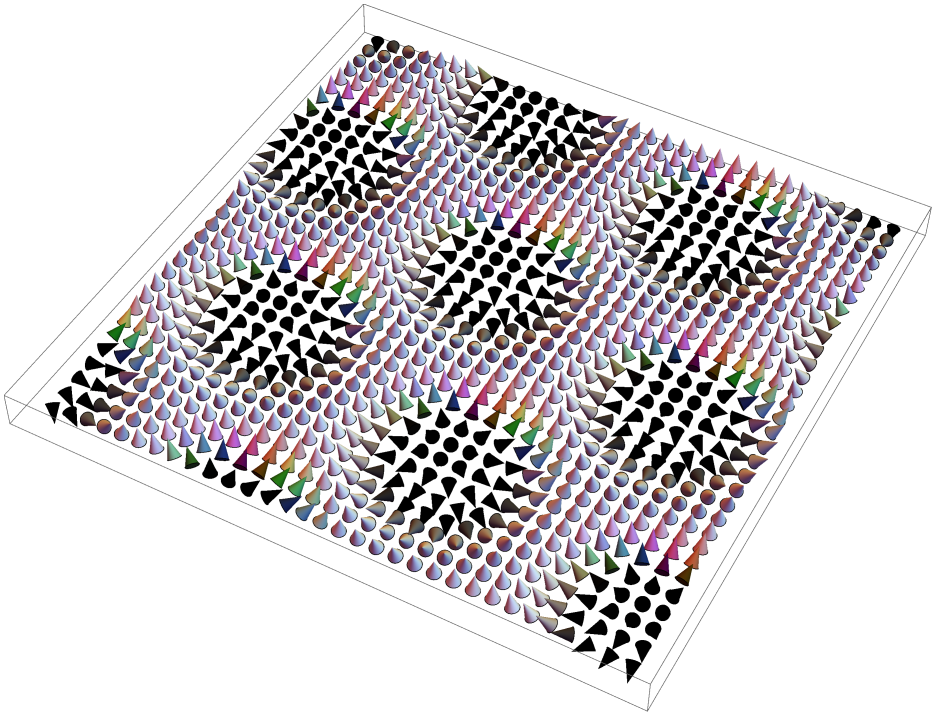

Supervised by:
Prof. Dr. **Rembert Duine**

December 2016

Institute for Theoretical Physics,
Leuvenlaan 4, 3584 CE Utrecht, The Netherlands

"I think nature's imagination Is so much greater than man's, she's never going to let us relax."

– Richard Feynman.

Abstract

Inspired by Onose *et al.* [1], who observed the thermal magnon Hall effect in pyrochlore ferromagnetic structures, the master Thesis in hand investigates the same effect of magnons in stable, rectangular, ferromagnetic [2] and antiferromagnetic [3] skyrmionic lattices. Our analysis is based on a Hamiltonian which consists of the following four terms: an exchange interaction, an easy axis anisotropy, the Dzyaloshinskii-Moriya interaction and an external magnetic field. Transformations on the initial Hamiltonian in order to obtain the non-interacting magnonic spin-wave Hamiltonian, and the standard method of diagonalisation, allow us to numerically compute the effective magnetic field that the magnons feel, which is essential ingredient to compute the transverse thermal conductivity.

The results found for both ferromagnetic and antiferromagnetic lattices show the presence of the Hall effect of magnons at low temperatures. Although a direct comparison between ferromagnets and antiferromagnets is impossible, since they differ in the size as well as in the number of skyrmions, we do compare the two configurations to conclude that the antiferromagnetic structure exhibits a stronger Hall effect.

Table of Contents

Preface

The Thesis in hand is the result of my 9-month effort for the partial fulfillment of the master degree in Theoretical Physics of Utrecht University.

The general layout of this Thesis has been constructed in such a way to form an as complete as possible guide to the topic of the magnon Hall effect to anyone who has some basic background in quantum mechanics and physics. Hence, in the beginning of Chapter 1, a short introduction to the Hall effect of charged particles is given. Then, the field of spintronics is introduced to give to the reader a basic idea what the topic is about, followed by the introduction to the notion of magnons, which are important in this work. Next, the thermal Hall effect is discussed and apart from this, the reader becomes familiar with some other important notions such as the Berry curvature, the Berry Phase and skyrmions. The mosaic of Chapter 1 is completed by a literature review, which consists of a discussion of relevant works of other people. The purpose of the literature review is twofold. On the one hand it reveals the uniqueness of this Thesis and on the other hand it connects it to previous works.

Chapter 2, firstly deals with the Hamiltonian used by paying particular attention at each term of it separately. Once the Hamiltonian has been discussed, the skyrmionic ground state of it, in both ferromagnets and antiferromagnets, is found. Then, both the procedures of finding the spin-wave Hamiltonian and the way of diagonalising it are briefly discussed. Since these methodologies are standard in literature, the appropriate references are provided for the reader who wants to read a rigorous mathematical explanation, which is outside of the scope of the Thesis. Once the Hamiltonian is written in the notion of second quantisation operators (spin-wave Hamiltonian), the procedure of extracting the transverse Hall conductivity follows. More specifically, the number of magnons is computed followed by two ways of computing the effective magnetic field.

In Chapter 3 the results found using the theory and the methodology of Chapter 2 are presented. In the beginning the dispersion relation of the Hamiltonian for the two different cases is numerically computed, then the average magnon occupation at each state is depicted in order to show the equivalence with Boson-Einstein statistics. After that, the distribution of the magnetic field is given in order to finish with the dependence of the thermal conductivity on temperature. The same procedure is followed for the antiferromagnetic case and finally, some comparisons and the conclusion of the Thesis is exported.

In Chapter 4 some open research questions and some possible extensions of the present Thesis are discussed. Some of them might be useful for my future research works and some others might inspire other people in order to continue working on the specific topic.

Finally, in the appendix, the reader can find a very short introduction to the ferromagnets and antiferromagnets, the derivation of magnon dispersion relation and the notion of chirality. All of these introductory physics contribute to the better understanding of the topic.

Having finished the tour over the chapter of my Thesis, I would like to thank my supervisor Prof. Dr. Rembert Duine because with his passion for spintronics, he subconsciously became my scientific role model and made me study hard in order to learn a lot of very interesting topics. Rick Keesman for giving me his numerical data and ultimately Jiansen Zheng and Patrick van Dieten for the very interesting discussions that helped me to understand the topic deeper.

Ilias Samathrakis
Utrecht, December 13, 2016

List of Figures

List of Tables

CHAPTER 1

Introduction

1.1 The Hall Effect

In this section, the Hall effect of charged particles is discussed, followed by the derivation of a simple expression for the Hall coefficient. Even though the Hall effect of charged particles is not the topic of the Thesis, it provides essential tools that we use throughout the project.

The Hall effect was discovered in 1879 by Edwin Hall. It has to do with the production of a voltage difference (known as the Hall voltage) across an electric conductor, transverse to the electric field and a magnetic field perpendicular to the current. A schematic representation of the Hall effect can be seen in Fig. 1.1.

In Fig. 1.1, the light blue area is the electric conductor, the green arrow points the voltage and the black one the direction of the magnetic field. Finally, the purple tube with the arrow shows the direction the electrons move.

As we can see in Fig. 1.1, electrons are restricted to move in (x, y) plane and the magnetic field is in the z-direction. A constant current flows in the x-direction. Hall effect states that this induces a voltage V_y in the y-direction. All these allow us to write:

1

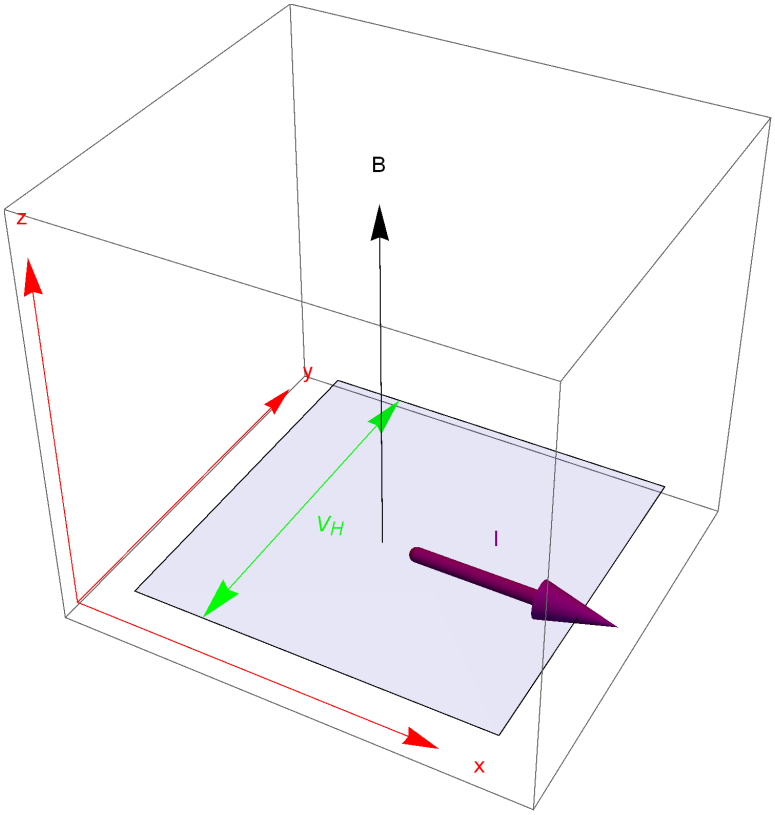

Figure 1.1: The presence of the magnetic field influences the motion of the electrons by forcing them to move in the y-direction. This effect is called the Hall effect.

$$\mathbf{B} = \begin{pmatrix} 0 \\ 0 \\ B \end{pmatrix}; \qquad \mathbf{E} = \begin{pmatrix} E_x \\ E_y \\ 0 \end{pmatrix}. \tag{1.1}$$

The equation of motion for a particle with mass m and charge e under the influence of the magnetic and electric field $\mathbf{B}$ and $\mathbf{E}$ respectively is:

$$m\frac{\partial \mathbf{v}}{\partial t} = -e\mathbf{E} - e\mathbf{v} \times \mathbf{B} - \frac{m}{\tau}\mathbf{v}; \tag{1.2}$$

where $\mathbf{v}$ is the velocity and τ the scattering time.

The first term on the right hand side is due to the electric field, the second one due to the magnetic field and the last one is a linear friction term that results from scattering of the electrons with impurities.

Eq. 1.2 is solved for $\mathbf{v}$ by considering equilibrium solutions that require $\frac{\partial \mathbf{v}}{\partial t} = 0$ in order to give:

$$
\begin{aligned}
v_x &= -\frac{e\tau}{m}\left(E_x + v_y B\right); \\
v_y &= -\frac{e\tau}{m}\left(E_y - v_x B\right); \\
v_z &= 0.
\end{aligned} \tag{1.3}
$$

Using the definitions for the current density and the cyclotron frequency:

$$
\begin{aligned}
\mathbf{J} &= -ne\mathbf{v}; \\
\omega_B &= \frac{eB}{m},
\end{aligned}
$$

with n the density of the charge carriers, we write Eq. 1.3 in matrix form as:

$$
\begin{pmatrix} 1 & \omega_B\tau \\ -\omega_B\tau & 1 \end{pmatrix} \begin{pmatrix} J_x \\ J_y \end{pmatrix} = \frac{e^2 n\tau}{m} \begin{pmatrix} E_x \\ E_y \end{pmatrix}. \tag{1.4}
$$

Ohm's law suggests that

$$
\mathbf{J} = \sigma\mathbf{E}, \tag{1.5}
$$

with σ the conductivity. So, Eq. 1.4 can be written as:

$$
\sigma = \frac{e^2 n\tau}{m} \frac{1}{1+\omega_B^2\tau^2} \begin{pmatrix} 1 & -\omega_B\tau \\ \omega_B\tau & 1 \end{pmatrix}. \tag{1.6}
$$

The off-diagonal elements of this the matrix in Eq. 1.6 are responsible for the Hall effect.

Multiplying both sides of Eq. 1.5 by σ^{-1} from the left and defining $\rho = \sigma^{-1}$ (the resistivity), we get:

$$
\mathbf{E} = \rho\mathbf{J}, \tag{1.7}
$$

which is in the same form as Eq. 1.4, so

$$\begin{pmatrix} E_x \\ E_y \end{pmatrix} = \begin{pmatrix} \rho_{xx} & \rho_{xy} \\ \rho_{yx} & \rho_{yy} \end{pmatrix} \begin{pmatrix} J_x \\ J_y \end{pmatrix} \Leftrightarrow \begin{pmatrix} E_x \\ E_y \end{pmatrix} = \begin{pmatrix} \frac{m}{e^2 n\tau} & \frac{\omega_B m}{e^2 n} \\ -\frac{\omega_B m}{e^2 n} & \frac{m}{e^2 n\tau} \end{pmatrix} \begin{pmatrix} J_x \\ J_y \end{pmatrix}. \tag{1.8}$$

The Hall coefficient is defined as $R_H = \frac{E_y}{BJ_x}$ evaluated in the limit $J_y \to 0$, so using Eq. 1.8 we write:

$$R_H = \frac{\rho_{xy}}{B} = \frac{\omega_B m}{Be^2 n} = \frac{1}{ne}. \tag{1.9}$$

From this results we see that the Hall coefficient does not depend on the scattering time. Therefore, the Hall effect is commonly used to experimentally determine the density of charge carriers.

1.2 Spintronics

As far as we know electrons have two fundamental properties: charge and spin. The first one has been measured and found equal to e and it has also been extensively studied the past decades in order to give some spectacular silicon based applications such as transistors. Most of these applications are based on the charge current, which unfortunately has some significant drawbacks [1]:

- The current is mediated by electrons, so some part of it is transferred to heat because of the dissipation and therefore is lost → the energy-efficiency drops.
- The electric charge has a specific unchanged value → not adjustable.
- Charge interactions (Coulomb interactions) are quite strong → interference problems.

A new generation of applications (for example data storage devices) may be constructed by using the other fundamental property of the electrons: spin. Spin is widely known as the property which specifies whether a particle is a boson or a fermion (integer or half-integer spin respectively) but it also has some other, non trivial, properties, such as becoming the information carrier of a system. A relatively new domain of physics which studies the "SPIN TRansport electrONICS", or shorter "spintronics", sets its goal not only to make useful applications by using the spin instead of the charge, but also to increase their efficiency. In this Thesis, wave-like spin excitations, called magnons, are used as the information carrier. The notion of magnon is presented in more details in the following section.

1.3 Magnons

The notion of magnon is necessary in order to proceed our tour in the very interesting world of the magnon Hall effect. In the present section, two ways of approaching magnons are discussed and the magnon dispersion relation is proven in the appendix. The first approach has to do with the classical way of understanding them, whereas the second one is purely quantum-mechanical.

The difficulty in understanding magnons arises from the fact that they are not "usual" particles; instead, they are quasi-particles, collective excitations of the electron's spin.

1. Semi-Classical approach:

   One way to understand the notion of magnons is to consider them as elementary excitations in ordered magnetic materials. Imagine an one-dimensional chain of spins (ferromagnetic case for simplicity); as the one presented in Fig. 1.2. The spins are orientated in the same upward direction and the system is at its ground state. If now a single spin in the middle of the chain is flipped, the system is not at its ground state anymore. Since this configuration is not energetically favourable, other spins will also deviate from their initial position in order to give rise to the lowest possible energy. In the end, the result is visible in Fig. 1.3. The deviation is propagating in a wave-form manner, forming spin waves (clear from the bottom part of Fig. 1.3). By using De Broglie's relations we can relate a particle to a wave and vise versa hence the quantised version of the spin wave is the so called magnon quasi-particle [9].

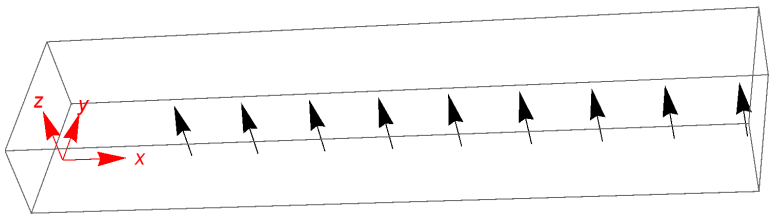

Figure 1.2: Chain of spins (ground state).

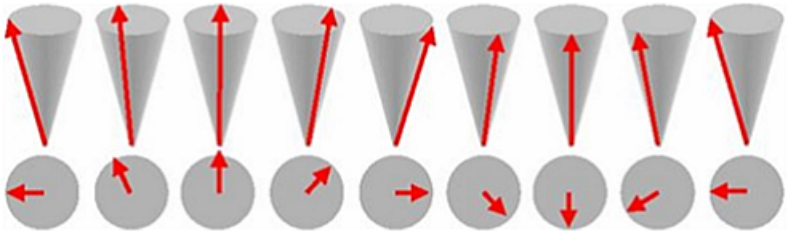

Figure 1.3: Spin waves (taken from [4]).

2. Quantum approach:

   Although the semi-classical approach explained before is simple, it is not accurate enough since spins have no classical analogues. The full quantum mechanical treatment requires the Holstein-Primakoff transformation which map the spin operators to bosonic creation and annihilation operators (create or annihilate a particle at a specific quantum state). In such a way, a spin wave can be thought of as one quantum of a spin reversal spread coherently over the system [10]. The interested reader can find the magnon dispersion relation in the appendix of the Thesis.

1.4 Thermal Hall Effect

In this chapter we argue that the Hall effect of neutral quasiparticles such as magnons exists and it is called Thermal Hall effect.

Magnons, as described in the previous section, are neutral quasiparticles. The question that arises is whether they can exhibit the Hall effect. The answer to this question is positive although they exhibit a different type of Hall effect dubbed "Thermal Hall effect". The basic difference between these two types is that in the latter one, particles do not experience a magnetic field in Lorentz force, instead, a temperature gradient ∇T transports a heat current $\mathbf{J}_Q$ [11]. The whole idea is illustrated in Fig. 1.4 (Fig. taken from [5]).

Magnons can travel in some magnetic configurations and pick up quantum-mechanical phases that are dubbed "Berry Phases", which give rise to "Berry Curvatures" that act as an effective magnetic field [7] that they can feel. These configurations should be skyrmionic in order to produce non vanishing Berry Curvatures.

The notions of "Berry Phase", "Berry Curvature" and "Skyrmion" follow in order to

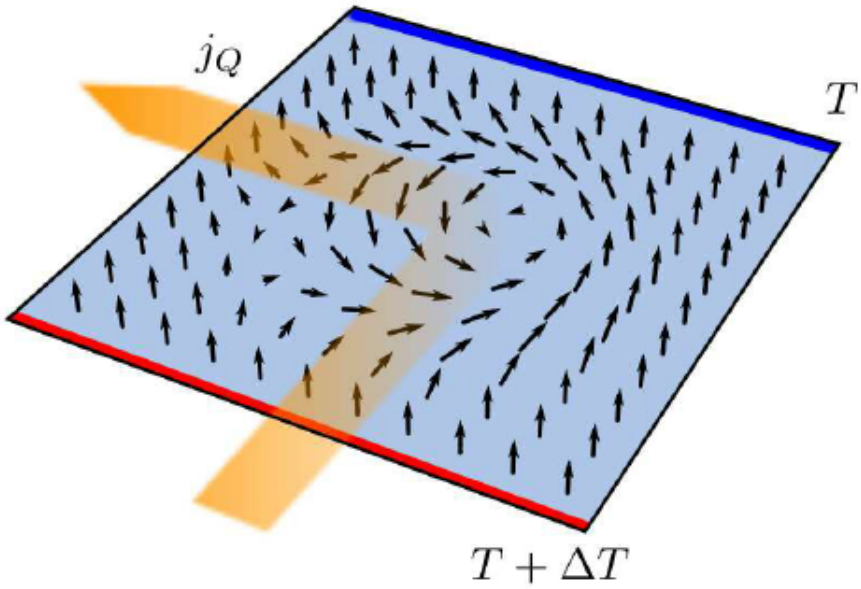

Figure 1.4: The presence of the temperature difference between the two sides transports heat current J_Q as indicated in the picture. This phenomenon is dubbed thermal Hall effect (taken from [5]).

give a clear picture of the effect to the reader.

1.4.1 Berry Phase

Before proceeding to the actual definition of the Berry phase, we present two classical examples to visualise it.

In Fig. 1.5, we can see the time zones of our planet. If we consider a specific time at a specific place and travel all around the Earth returning at the same place, we can see that the time depends on the chosen direction. In this example, moving to the east will make you "gain" one day at the end, the opposite will happen if you move to the west. Another example is depicted in Fig. 1.6, where a specific vector changes its orientation after completing a circle as the one depicted. In this case, the equivalence of the Berry phase is called "anholonomy angle" and it is equal to the solid angle Ω of the sphere. The analytic calculation can be found in [8].

A quantum version of the Berry phase can be understood with the Aharonov-Bohm effect. An electron beam is moving towards a solenoid, similar to the one depicted in Fig. 1.7 and it splits in two at some distance before reaching it. The two beams follow different paths around the solenoid, which are denoted by C_1 and C_2, before being recombined. The phase difference of the two beams is computed in two different situations inside the solenoid:

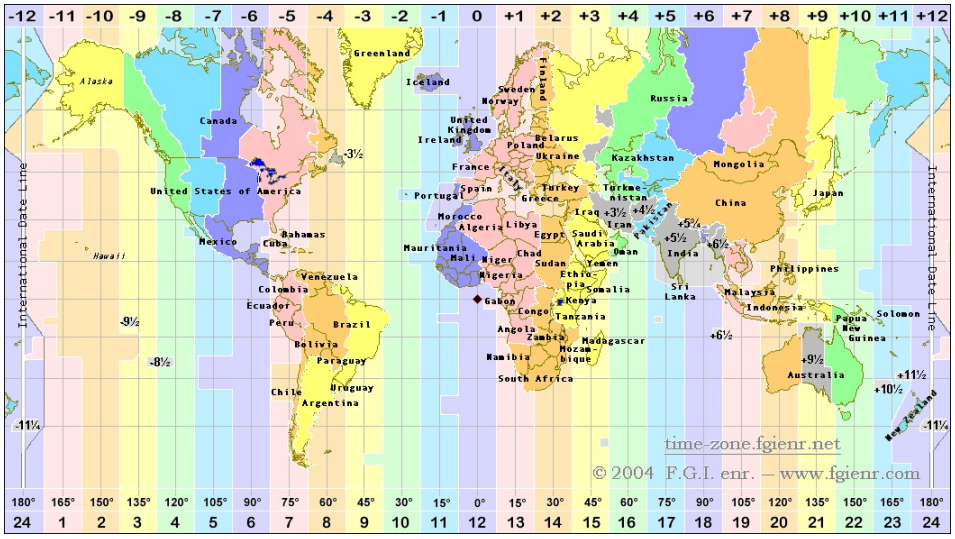

Figure 1.5: Time Zones (taken from [6]).

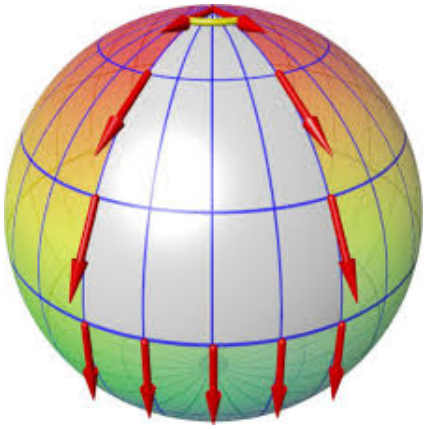

Figure 1.6: Parallel Transport (taken from [7]).

- $\underline{\mathbf{B} = 0}$

In this case the wave functions ψ_i of the beams are given by plane waves of the form:

$$\begin{aligned} \psi_1 &= Ae^{ikx_1}; \\ \psi_2 &= Ae^{ikx_2}. \end{aligned} \tag{1.10}$$

Hence the phase difference is:

$$\Delta\Phi = k\left(x_1 - x_2\right), \tag{1.11}$$

and the interference pattern only depends on the difference between the travel paths of the two beams.

- $\underline{\mathbf{B} \neq 0}$

  In this case the wave functions ψ_i acquire additional phases due to the presence of the magnetic field inside the solenoid.

$$\begin{aligned} \psi_1 &= e^{ig_1(r)}\psi_1 = Ae^{ikx_1+ig_1(r)}; \\ \psi_2 &= e^{ig_2(r)}\psi_2 = Ae^{ikx_2+ig_2(r)}. \end{aligned} \tag{1.12}$$

  Hence the phase difference is:

$$\begin{aligned} \Delta\Phi &= k\left(x_1 - x_2\right) + g_1\left(\mathbf{r}\right) - g_2\left(\mathbf{r}\right) \\ &= k\left(x_1 - x_2\right) + \frac{e}{\hbar}\left[\int_{C_1} \mathbf{A}\left(\mathbf{r}^{'}\right)\cdot d\mathbf{r}^{'} - \int_{C_2} \mathbf{A}\left(\mathbf{r}^{'}\right)\cdot d\mathbf{r}^{'}\right] \\ &= k\left(x_1 - x_2\right) + \frac{e}{\hbar}\oint_{C} \mathbf{A}\left(\mathbf{r}^{'}\right)\cdot d\mathbf{r}^{'} \\ &= k\left(x_1 - x_2\right) + \frac{e\Phi_m}{\hbar}, \end{aligned} \tag{1.13}$$

  and the phase difference depends both on the magnetic flux (Φ_m) inside the solenoid and on the difference of the optical paths of the two beams. This effect is known as the Aharonov-Bohm effect and the phase acquired as Berry phase.

Three examples (two classical and one quantum) have been discussed in order to give a flavour of the notion of the "Berry phase" to the reader. The actual definition of it, that holds for any system follows.

Definition: "A quantal system in an eigenstate, slowly transported round a circuit C by varying parameters $\mathbf{X}$ in its Hamiltonian $\hat{H}(\mathrm{X})$, will acquire a geometrical phase factor $\exp\{i\gamma(\mathrm{C})\}$ in addition to the familiar dynamical phase factor."

The quantity $\gamma(\mathrm{C})$ is known as the Berry phase and it is mathematically defined as:

$$\gamma(\mathrm{C}) = \oint_{C} i\langle\psi_n|\nabla|\psi_n\rangle\cdot d\mathbf{X}, \tag{1.14}$$

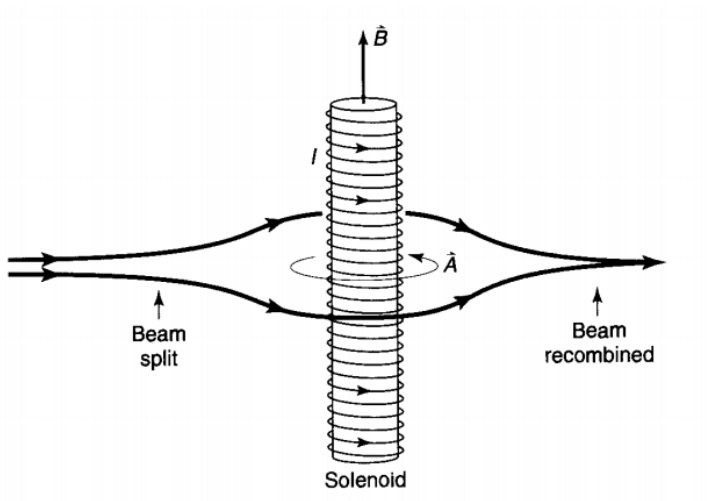

Figure 1.7: The phase difference between the two beams depends on the magnetic flux inside the solenoid when the magnetic field is turned on. This effect is known as the Aharonov-Bohm Effect (taken from [8]).

where ψ_n is the n^{th}-eigenstate of the Hamiltonian $\hat{H}(\mathrm{X})$.

The interested reader can find more information about the Aharonov-Bohm effect in [12].

1.4.2 Berry Curvature

Berry phase was defined in section 1.4.1 and more specifically from Eq. 1.14. A closer look to the mathematical definition of the Berry phase, will reveal its strangeness. The Berry phase itself (left hand side of the definition) is a meaningful quantity, which can be observed experimentally. However, the integrand (which is called the Berry connection) seems arbitrary and without any physical meaning [12]. In order to overcome this problem, we can think of our Berry connection as of an abstract vector potential $\mathbf{A}_n(\mathbf{X})$ known as the Berry vector potential. The definition of the Berry phase now becomes:

$$\gamma(\mathrm{C}) = \oint_C \mathbf{A}_n(\mathbf{X}) \cdot d\mathbf{X}. \tag{1.15}$$

Stokes' theorem allows us to write:

$$\gamma(\mathrm{C}) = -\iint \mathbf{B}(\mathbf{X}) \cdot \mathbf{n}\, d\sigma, \tag{1.16}$$

where the B-field is defined as:

$$\mathbf{B}_n(\mathbf{X}) = \nabla \times \mathbf{A}_n(\mathbf{X}), \tag{1.17}$$

and it is an observable quantity in the electromagnetic theory.

In the general case now, let us symbolise Berry connection with χ_n, such that:

$$\chi_n = i\langle\psi_n|\nabla|\psi_n\rangle. \tag{1.18}$$

The analogue of the magnetic field now is given by an antisymmetric tensor field called curvature (Berry curvature in this case).

$$\mathbf{\Omega}_{\mu\nu}(\mathbf{X}) = \partial_{X^\mu}\chi^n_\nu - \partial_{X^\nu}\chi^n_\mu, \tag{1.19}$$

which gives rise to:

$$\mathbf{\Omega}_n(\mathbf{X}) = \nabla \times \chi(X). \tag{1.20}$$

The quantity Ω is called Berry curvature.

1.4.3 Skyrmions

Since the configurations needed to produce non vanishing Berry curvature are skyrmionic, the notion of skyrmion is introduced.

The notion of "skyrmions" can be easier understood if we first introduce the "topological charge" or "Skyrmion number" as:

$$n = \frac{1}{4\pi}\int \mathbf{M}\cdot\left(\frac{\partial\mathbf{M}}{\partial x}\times\frac{\partial\mathbf{M}}{\partial y}\right)dx\,dy, \tag{1.21}$$

where $\mathbf{M}$ is the unit spin direction vector.

A simple one-dimensional example to visualise the topological charge is given in Fig. 1.8. In the upper left part of that figure, the initial orientation of the chain (with black), the orientation of the twists (with blue) and the intermediate orientation

(with red) are presented. As it is clear, the twist does not rotate over 360 degrees. Unlike the upper part, the bottom chain is rotated over 360 degrees. The progressive result of both chains are depicted in the right part of Fig. 1.8. In the first case we observe $n_1 = 0$, whereas in the second one $n_2 = 1$.

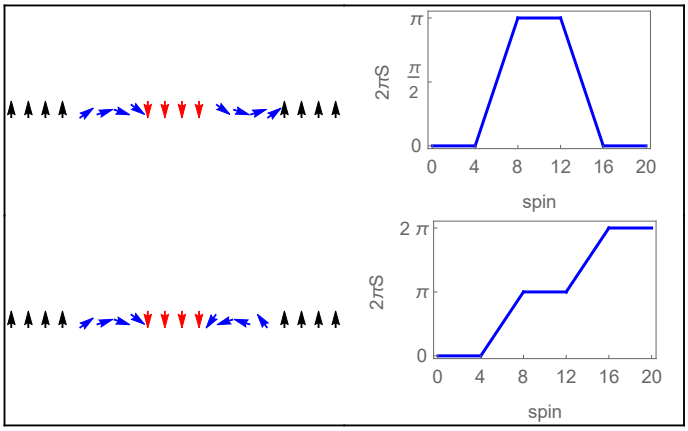

Figure 1.8: Domain walls and skyrmion number.

The value of the topological charge "n" characterises if a configuration is a skyrmion or not. More specifically, a configuration for which "n" takes a non vanishing and integer value is called skyrmion [13].

An example of a two-dimensional skyrmion in a spin lattice can be seen in Fig. 1.9. It has to be mentioned that these "constructions" are energetically favourable in some materials (as discussed in more detail further on) which means that they are stable as well. Muhlbauer *et al.* [2] found the magnetic phases of $MnSi$ and their results show evidence for the stability of the Skyrmionic phase in a magnetic material (see Fig. 1.10).

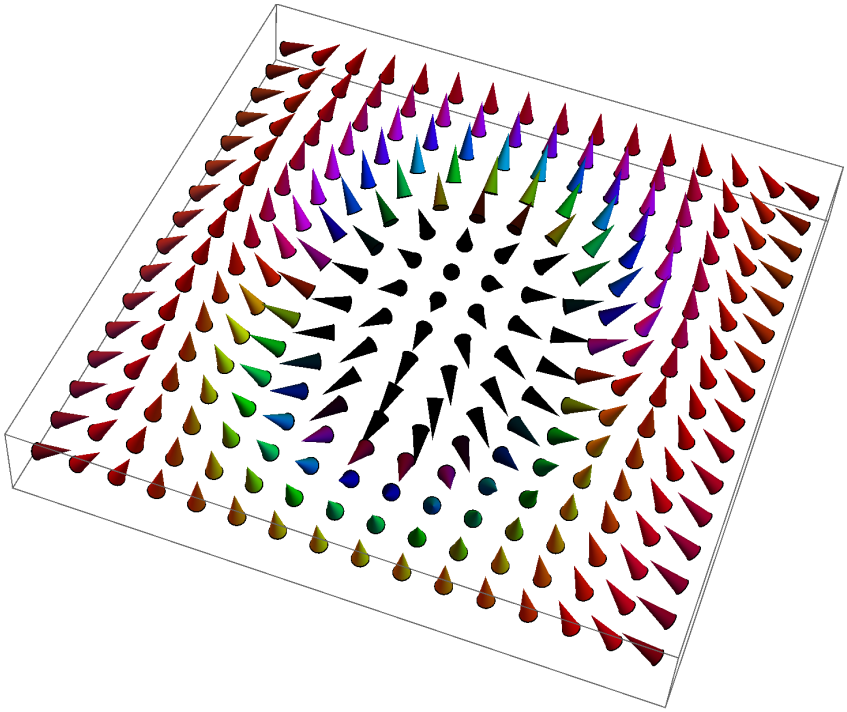

Figure 1.9: A ferromagnetic Skyrmion.

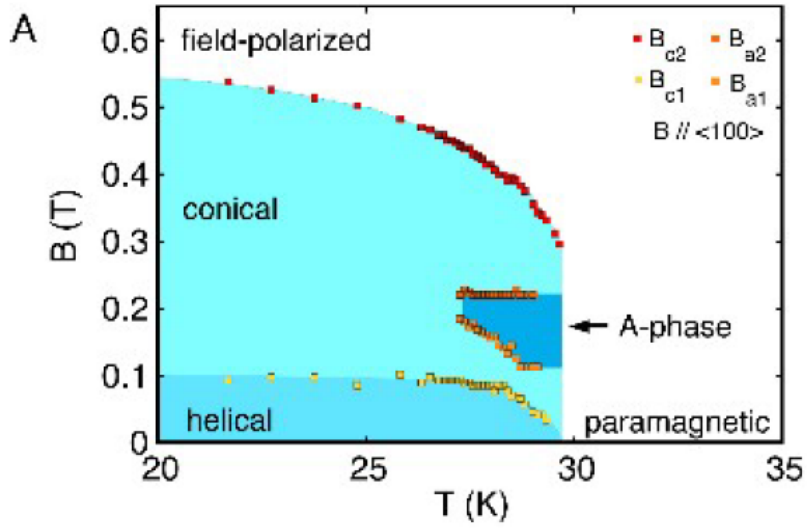

Figure 1.10: Magnetic phases of $MnSi$. The A-phase corresponds to the Skyrmion phase (taken from [2]).

Mathematically speaking, skyrmions are examples of a specific class of solitons that cannot decay due to topological protection. Solitons are a certain type of solutions of several partial differential equations such as the Sine-Gordon and the Landau-Lifshitz that are given respectively by:

$$\frac{\partial^2 u\left(x,t\right)}{\partial t^2} - \frac{\partial^2 u\left(x,t\right)}{\partial x^2} + \sin u\left(x,t\right) = 0; \tag{1.22}$$

$$\frac{d\mathbf{M}}{dt} = -\gamma \mathbf{M} \times \mathbf{H}_{eff} - \lambda \mathbf{M} \times \left(\mathbf{M} \times \mathbf{H}_{eff}\right).$$

One can think of solitons as wave packets that move through a dispersive and nonlinear medium, while changing neither their shape nor their velocity [14].

1.5 Literature Review

In this section, the work that has already been done is summarised and the uniqueness of the work presented in this Thesis is stressed.

In order to be able to investigate the thermal Hall effect of magnons in skyrmionic structures, we first have to prove that:

- Magnon spin current indeed exists, which means that magnons can be used as information carriers.
- Skyrmionic structures that are going to be used as the initial configuration both exist and they are stable.

Hence, the scientific progress in these two topics (information carrier and in lattices) is relevant to the present Thesis and therefore it is discussed.

Information Carrier:

As explained in section 1.2 charge has some significant drawbacks in being the carrier of information. The same holds for spins mainly because it is a property of electrons. In recent year though, another candidate has dramatically increased its awareness of becoming the information carrier; and this is the magnon, the current of which has been shown to be possible by means of the spin Seebeck effect as explained by Uchida *et al.* [15] and in the spin Hall effect as explained by Kajiwara *et al.* [16]. Magnons are probably better suited candidates since they are less subject to heating and furthermore because its quasiparticle bosonic nature allows us to ignore losses due to scattering phenomena at least at low temperatures, as Meier *et al.* have shown [17].

Lattice:

Muhlbauer *et al.* [2] have shown that ferromagnetic Skyrmionic structures are stable in $MnSi$ (phase A in their diagram, which is also mentioned in subsection 2.4). Furthermore, Onose *et al.* [1] have observed the magnon Hall effect in ferromagnetic surfaces by using the configuration of Fig. 1.11. Regarding antiferromagnets, Keesman *et al.* [3] have shown that there are stable antiferromagnetic skyrmionic structures under some specific conditions and that they are easier to control in a sense that their skyrmions move faster, which was shown by Barker and Tretiakov [18]

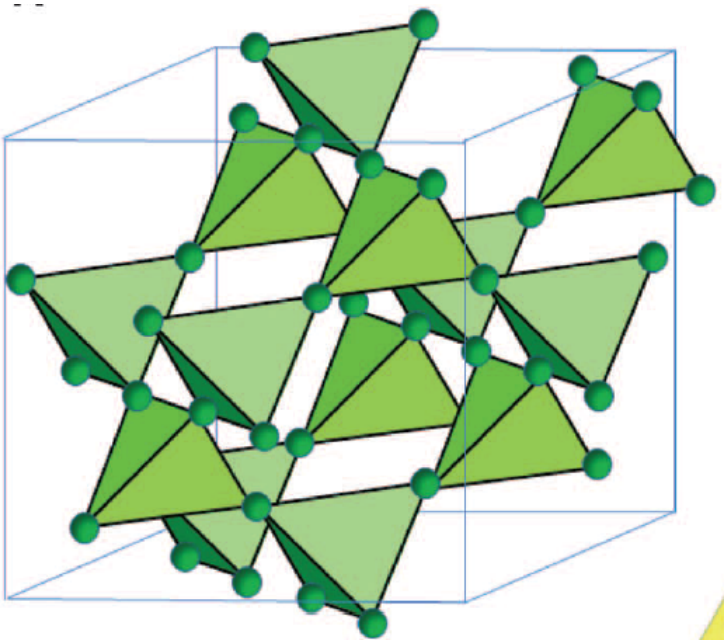

Figure 1.11: The crystal structure of $Lu_2V_2O_7$ (taken from [1]).

To conclude, the master Thesis in hand deals with the thermal Hall effect of magnons in some specific stable skyrmionic ferromagnetic and antiferromagnetic structures. In other words, the possibility of using spin quasiparticles (magnons) as the information carrier of a system and compute their transverse thermal conductivity to find whether they can exhibit the Hall effect is investigated.

CHAPTER 2

Methodology

In this section the methodology followed to obtain the final results is discussed. The Hamiltonian is first introduced and each term of it is analysed. Then, the ground state which will be used as the initial configuration is given. Next, the methodology of finding the spin-wave Hamiltonian, which involves some transformations, follows. Thereafter, the standard method of diagonalising Hamiltonians of these type is briefly discussed (the quick reader can skip subsection 2.5). Finally, a detailed explanation of the procedure of the Hall conductivity was computed is presented.

2.1 Theoretical Description: the Hamiltonian

The system under consideration is a magnetic system, hence the energy is determined by the interactions of the spins. In addition to these interactions, an external magnetic field contributes as well. Therefore, the Hamiltonian takes the form:

$$H = H_{int} + H_{ext}, \tag{2.1}$$

where the subscripts "int" and "ext" correspond to the internal and the external contribution respectively.

- Internal Part:
  The internal part of the Hamiltonian is due to the spin interaction among

particles. In general it reads:

$$H_{int} = \sum_{i,j} \mathbf{S}_i^T \mathbf{V}_{ij} \mathbf{S}_j, \tag{2.2}$$

with $\mathbf{V}_{ij}$ the interaction matrix given by:

$$\mathbf{V}_{ij} = \begin{pmatrix} V_{11}^{ij} & V_{12}^{ij} & V_{13}^{ij} \\ V_{21}^{ij} & V_{22}^{ij} & V_{23}^{ij} \\ V_{31}^{ij} & V_{32}^{ij} & V_{33}^{ij} \end{pmatrix}. \tag{2.3}$$

- External Part:
  The external part is only due to the presence of the external magnetic field and its contribution to the Hamiltonian is:

$$H_{ext} = B \sum_i (\mathbf{S}_i)^z. \tag{2.4}$$

In order to simplify the interaction matrix $\mathbf{V}_{ij}$ of the internal part of the Hamiltonian, we can write it as follows [19, 20]:

$$\mathbf{V}_{ij} = J_{ij} + \mathbf{V}_{ij}^{+} + \mathbf{V}_{ij}^{-}, \tag{2.5}$$

where J_{ij} is the exchange term, $\mathbf{V}_{ij}^{+}$ is the anisotropic exchange (symmetric, traceless) and $\mathbf{V}_{ij}^{-}$ is the Dzyaloshinskii-Moriya interaction (antisymmetric). Each of these terms contributes differently to the Hamiltonian and further analysis is provided in the following subsections.

2.1.1 Heisenberg Model

The first term on the right hand side of Eq. 2.5 is defined as (taken from [19]):

$$J_{ij} = \frac{Tr\left(\mathbf{V}_{ij}\right)}{3}, \tag{2.6}$$

which corresponds to the isotropic part of the interaction matrix and it is called "exchange integral".

The Heisenberg model is the simplest model that can mathematically describe spin interactions quantum mechanically and it is present in all magnetic systems. The general form of the Hamiltonian is:

$$H_{gen} = -\sum_{i \neq j} J_{ij} \mathbf{S}_i \cdot \mathbf{S}_j. \tag{2.7}$$

In our case there are two additional restrictions that simplify this term.

- The interactions between particles have no preference in the direction, which practically means that J_{ij} can be simply written as J (it does not depend on the indices).
- There are only interactions between nearest neighbouring sites. This is mathematically expressed by the sum $\sum_{\langle i,j \rangle}$.

Under these conditions the Hamiltonian is:

$$H_{HM} = -J \sum_{\langle i,j \rangle} \mathbf{S}_i \cdot \mathbf{S}_j. \tag{2.8}$$

The interested reader can find more information and the complete derivation of the exchange term [21].

2.1.2 Anisotropy Term

The second term on the right hand side of Eq. 2.5 is defined as (taken from [19]):

$$\mathbf{V}_{ij}^{+} = \frac{\mathbf{V}_{ij} + \mathbf{V}_{ij}^{T}}{2} - J_{ij}, \tag{2.9}$$

which corresponds to a symmetric traceless part and it is called "anisotropic exchange".

Unlike the exchange integral of the previous subsection, the anisotropic exchange has a minor contribution and it is computationally demanding, therefore only an important part of it will be taken into account and the rest will be neglected.
The important part is the on-site term $\mathbf{V}_{ii}^{+}$ hence, the Hamiltonian reads:

$$H_A = \sum_i \mathbf{S}_i^T \mathbf{K}_i \mathbf{S}_i, \tag{2.10}$$

with $\mathbf{K}_i$ the lattice anisotropy tensor.

As in the previous subsection, there are two additional simplifications that make the term easier.

- The lattice anisotropy tensor $\mathbf{K}_i$ is the same at any position of the lattice.
- The anisotropy only exists in the z-direction.

Under these simplifications the Hamiltonian can be written in an easier way as:

$$H_A = -K \sum_i \left(\mathbf{S}_i^2\right)^z . \tag{2.11}$$

2.1.3 Dzyaloshinskii-Moriya Interaction

The third term on the right hand side of Eq. 2.5 is defined as (taken from [19]):

$$\mathbf{V}_{ij}^- = \frac{\mathbf{V}_{ij} - \mathbf{V}_{ij}^T}{2}, \tag{2.12}$$

which corresponds to the antisymmetric part of the interaction matrix.

Since $\mathbf{V}_{ij}^-$ is by definition antisymmetric, we can express it as a Three-dimensional vector, using the formula:

$$\left(\mathbf{V}_{ij}^-\right)_{mn} = \sum_{l=1}^{3} D_l^{ij} \epsilon_{lmn}, \tag{2.13}$$

with ϵ_{lmn} to be the Levi-Civita symbol and $\mathbf{D}^{ij}$ the Dzyaloshinskii vector. So:

$$H_{DMI} = \sum_{\langle i,j \rangle} \mathbf{S}_i^T \mathbf{V}_{ij}^- \mathbf{S}_j = \sum_{\langle i,j \rangle} \mathbf{D}_{i,j} \cdot \left(\mathbf{S}_i \times \mathbf{S}_j\right). \tag{2.14}$$

This term is based on chiral symmetries [22] since the Dzyaloshinskii vector vanishes when the system faces inversion symmetry [21] and it was initially derived by Dzyaloshinskii in 1960. It also theoretically explains the phase A in Fig.1.10. After Moriya's contribution the term has been named as the Dzyaloshinskii-Moriya spin-orbit interaction which is one of the ways to create Skyrmions [23]. Further analysis will reveal that this term tries to force $\mathbf{S}_i$ and $\mathbf{S}_j$ to be at a right angle in a plane perpendicular to the vector $\mathbf{D}$.

An important simplification that makes this term much easier is to assume that the amplitude of the interaction is the same regardless the direction. This does not mean

though that the vector $\mathbf{D}_{ij}$ points always to the same direction. The Dzyaloshinskii vector $\mathbf{D}_{ij}$ that we consider in this Thesis is given by:

$$\mathbf{D}_{ij} = \begin{cases} (0, D, 0) & \text{if } j \text{ is the "left" neighbour of } i \\ (0, -D, 0) & \text{if } j \text{ is the "right" neighbour of } i \\ (D, 0, 0) & \text{if } j \text{ is the "above" neighbour of } i \\ (-D, 0, 0) & \text{if } j \text{ is the "below" neighbour of } i \end{cases}; \tag{2.15}$$

where D is the Dzyaloshinskii-Moriya coupling.

2.1.4 External Magnetic Field

As explained before, the external part of the Hamiltonian is only due the the presence of the magnetic field. This magnetic field stabilises the configuration and it is also responsible for the Zeeman effect. In this Thesis, it has been taken parallel to the z-direction ($\mathbf{B} = B\hat{z}$).

2.2 Full Hamiltonian

As it has become clear, the full Hamiltonian will be given by the sum of all the previously mentioned parts.

$$H = H_{HM} + H_A + H_{DMI} + H_{ext}. \tag{2.16}$$

Therefore:

$$H = -J \sum_{\langle i,j \rangle} \mathbf{S}_i \cdot \mathbf{S}_j - K \sum_i \left(\mathbf{S}_i^2\right)^z + \sum_{\langle i,j \rangle} \mathbf{D}_{i,j} \cdot (\mathbf{S}_i \times \mathbf{S}_j) - B \sum_i \left(\mathbf{S}_i\right)^z. \tag{2.17}$$

2.3 The Ground State

Onose *et al.* [1] used the pyrochlore ferromagnetic structure of $Lu_2V_2O_7$ in order to observe the thermal magnon Hall effect. In this Thesis, the shape of the ground state used is simpler. A two-dimensional lattice with dimensions $L_x = 16$ and $L_y = 16$ with periodic one-side boundary conditions for the ferromagnets and a 32×32 with full periodic boundary conditions for the antiferromagnets have been used. Fig. 2.1 illustrates the shape of the initial configuration for both cases (the total number of spins is different). Each lattice site at this figure corresponds to the initial point of the three-dimensional spin vector.

$(L_y-1)\,L_x+1$	$(L_y-1)\,L_x+2$	$(L_y-1)\,L_x+3$	$\cdots$	L_yL_x
$\vdots$	$\vdots$	$\vdots$	$\iddots$	$\vdots$
$2L_x+1$	$2L_x+2$	$2L_x+3$	$\cdots$	$3L_x$
L_x+1	L_x+2	L_x+3	$\cdots$	$2L_x$
1	2	3	$\cdots$	L_x

Figure 2.1: Initial lattice.

Given specific values to the couplings in the Hamiltonian of Eq. 2.17, the ground states were found using Monte Carlo Simulations performed by R. Keesman. In the following part of this section, two ways of visualising the ground states will be given. In the first one each spin vector is coloured in respect to its direction whereas in the second one each spin vector at each lattice point is associated to a colour in such a way the the deviations from the plane are determined according to the given colour explanation adjacent to the figure.

Ferromagnets:

For the values of couplings shown in Table 2.1, the ground state has one skyrmion.

Coupling Constant	Numerical Value $\left[\lvert J\rvert\right]$
J	1.0
D	0.598833
K	0.0
B	0.1793

Table 2.1: Ground state coupling constants of Hamiltonian in Eq. 2.17 for ferromagnets. The coupling constants are in units of $|J|$.

Keesman *et al.* [24] showed that this skyrmionic ground state is stable. The two different ways of visualising this configurations, as explained before, are shown in Fig. 2.2 and Fig. 2.3. respectively.

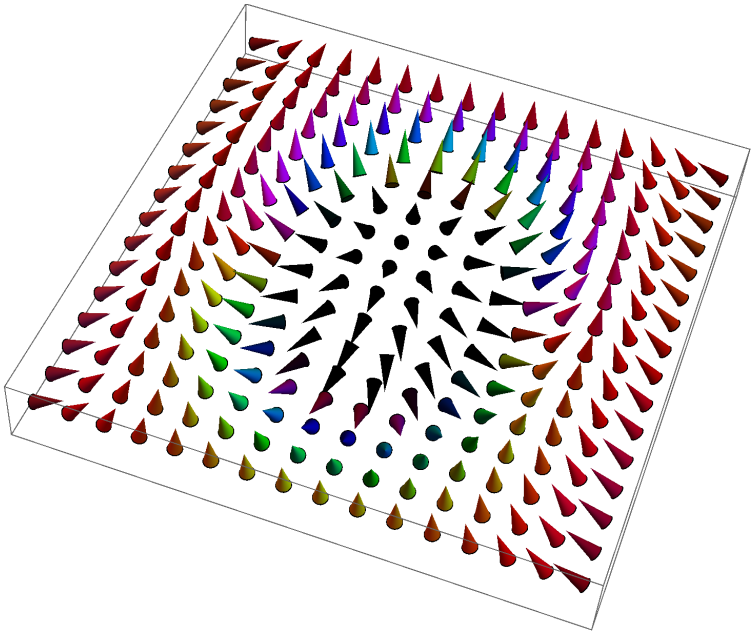

Figure 2.2: The ferromagnetic Skyrmionic ground sate in three-dimensions.

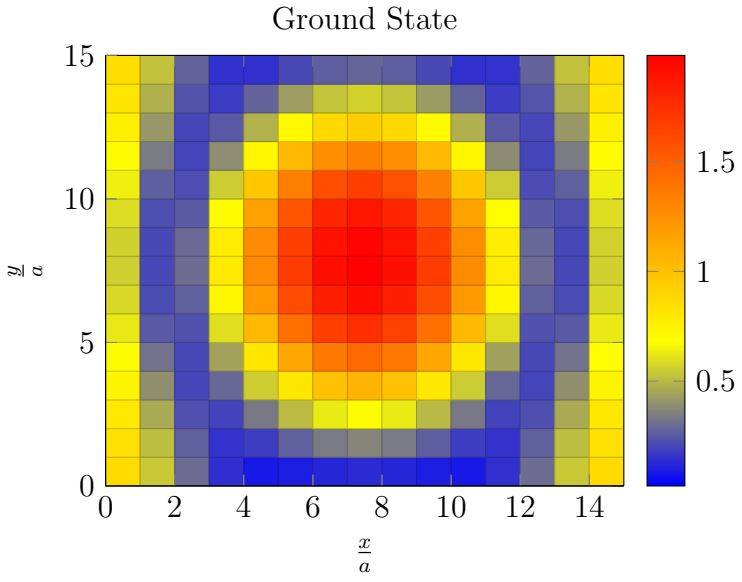

Figure 2.3: The ferromagnetic Skyrmionic ground sate in two-dimensions.

Antiferromagnets:

Regarding the antiferromagnetic case, the couplings that give rise to an eight-skyrmion ground state are given in Table 2.2.

Coupling Constant	Numerical Value $[\lvert J\rvert]$
J	-1.0
D	0.760216
K	0.0
B	3.2

Table 2.2: Ground state coupling constants of Hamiltonian 2.17 in antiferromagnets. The coupling constants are in units of $|J|$

The stability is proven by Keesman *et al.* [3]. Similarly to the ferromagnetic case, the two ways of visualisation are shown in Fig. 2.4 and Fig. 2.5 respectively.

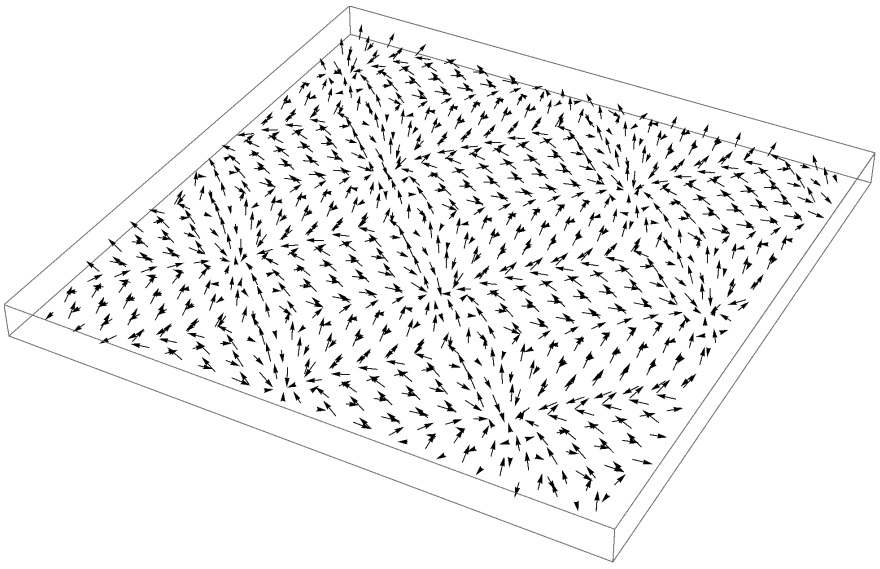

Figure 2.4: The antiferromagnetic Skyrmionic ground sate in three-dimensions.

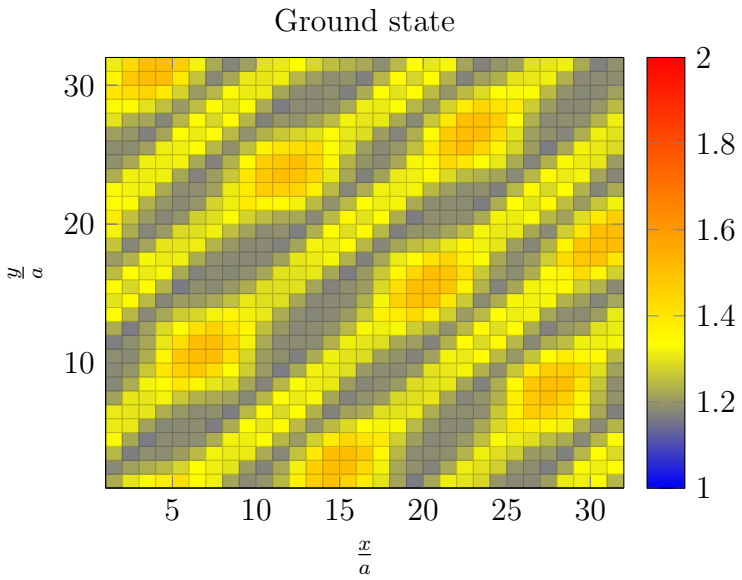

Figure 2.5: Two-dimensional visualisation of the antiferromagnetic Skyrmionic ground state.

2.4 Spin-wave Hamiltonian: Transformations

The Hamiltonian in Eq. 2.17 depends on the spin vectors $\mathbf{S}_i$. However, if the Hamiltonian transforms in such a way that it depends on some creation and annihilation operators (spin-wave, second quantised form), its treatment becomes much easier. In order to get to that result we follow a specific procedure of transformations, which, due to the presence of the Skyrmions, are not straightforward. The method consists of two major steps that are going to be presented in some detail. The first step involves a local frame rotation that orientates the z-axis at each position in such a way to be parallel to the direction of the spin in ground state and the second one the mapping to bosonic operators [25].

1. In spherical coordinates, the spin vector at each site is defined from the following vector:

$$\Omega_i = \begin{pmatrix} \sin\theta_i \cos\phi_i \\ \sin\theta_i \sin\phi_i \\ \cos\theta_i \end{pmatrix}; \tag{2.18}$$

where θ_i and ϕ_i are the Euler angles.

Since the spin waves are small deviations from the ground state of each spin vector $\mathbf{S}_i$, we can use a local frame to refer to each of them. Therefore,

multiplying each spin vector by a rotation matrix U is required [26].

$$\bar{\mathbf{S}}_i = U_i \mathbf{S}_i. \tag{2.19}$$

This rotation matrix U in terms of the Euler angles is given by:

$$U_i = \begin{pmatrix} \cos\theta_i \cos\phi_i & \cos\theta_i \sin\phi_i & -\sin\theta_i \\ -\sin\phi_i & \cos\phi_i & 0 \\ \cos\phi_i \sin\theta_i & \sin\theta_i \sin\phi_i & \cos\theta_i \end{pmatrix}. \tag{2.20}$$

For future reference, we compute the inverse matrix, which reads:

$$U_i^{-1} = \begin{pmatrix} \cos\theta_i \cos\phi_i & -\sin\phi_i & \cos\phi_i \sin\theta_i \\ \cos\theta_i \sin\phi_i & \cos\phi_i & \sin\theta_i \sin\phi_i \\ -\sin\theta_i & 0 & \cos\theta_i \end{pmatrix}. \tag{2.21}$$

Plugging Eq. 2.19 in the Hamiltonian 2.17, we get:

$$\begin{aligned} H = &-J \sum_{\langle i,j \rangle} \bar{\mathbf{S}}_i \cdot U_i U_j^{-1} \bar{\mathbf{S}}_j - K \sum_i \left(U_i^{-1} \bar{\mathbf{S}}_i\right)_z^2 \\ &- B \sum_i \left(U_i^{-1} \bar{\mathbf{S}}_i\right)_z + \sum_{\langle i,j \rangle} \bar{\mathbf{D}}_{i,j} \cdot \left[\left(U_i^{-1} \bar{\mathbf{S}}_i\right) \times \left(U_j^{-1} \bar{\mathbf{S}}_j\right)\right]; \end{aligned} \tag{2.22}$$

which is more compactly written as:

$$\begin{aligned} H = &-\frac{1}{2} \sum_{i \neq j} J F_{ij}^{\alpha\beta} \bar{S}_{i\alpha} \bar{S}_{j\beta} + \frac{1}{2} \sum_{i \neq j} D_\gamma^{ij} G_{ij}^{\gamma\alpha\beta} \bar{S}_{i\alpha} \bar{S}_{j\beta} \\ &+ K \sum_i G_i^{z\alpha} G_i^{z\beta} \bar{S}_{i\alpha} \bar{S}_{i\beta} - B \sum_i G_i^{z\alpha} \bar{S}_{i\alpha}. \end{aligned} \tag{2.23}$$

In the Hamiltonian 2.23, $G_{ij}^{\gamma\alpha\beta}$ are given by:

$$\begin{aligned} G_{ij}^{x\alpha\beta} &= G_i^{y\alpha} G_j^{z\beta} - G_i^{z\alpha} G_j^{y\beta}; \\ G_{ij}^{y\alpha\beta} &= G_i^{x\alpha} G_j^{z\beta} - G_i^{z\alpha} G_j^{x\beta}; \\ G_{ij}^{z\alpha\beta} &= G_i^{x\alpha} G_j^{y\beta} - G_i^{y\alpha} G_j^{x\beta}, \end{aligned} \tag{2.24}$$

and $G_i^{\alpha\beta}$ from:

$$U_i^{-1} = \begin{pmatrix} G_i^{xx} & G_i^{xy} & G_i^{xz} \\ G_i^{yx} & G_i^{yy} & G_i^{yz} \\ G_i^{zx} & G_i^{zy} & G_i^{zz} \end{pmatrix}. \tag{2.25}$$

Furthermore, $F_{ij}^{\alpha\beta}$ from:

$$U_i U_j^{-1} = \begin{pmatrix} F_{ij}^{xx} & F_{ij}^{xy} & F_{ij}^{xz} \\ F_{ij}^{yx} & F_{ij}^{yy} & F_{ij}^{yz} \\ F_{ij}^{zx} & F_{ij}^{zy} & F_{ij}^{zz} \end{pmatrix}. \tag{2.26}$$

2. So far, Hamiltonian 2.23 is written in terms of the local frame used, although it is not yet a function of creation and annihilation operators $a^\dagger$ and a. Using first the relations between the components of the spin vector and the spin creation and annihilation operators, which are the following:

$$\begin{aligned} \bar{S}_x &= \tfrac{\bar{S_+}+\bar{S_-}}{2}; \\ \bar{S}_y &= \tfrac{\bar{S_+}-\bar{S_-}}{2i}, \end{aligned} \tag{2.27}$$

allows us to map the spin operators $\bar{\mathbf{S}}_\pm$ to bosonic annihilation and creation operators a and $a^\dagger$ respectively by using the Holstein-Primakoff transformations [27]. These transformations were Taylor-expanded up to the first order to give Eq. 2.28. The expansion holds if $\frac{1}{\bar{S}} \ll 1$ which means that $\bar{S} \gg 1$.

$$\begin{aligned} \bar{S_+} &= \hbar\sqrt{2\bar{S}}\sqrt{1-\tfrac{a^\dagger a}{2\bar{S}}}\; a \simeq \hbar\sqrt{2\bar{S}}\; a; \\ \bar{S_-} &= \hbar\sqrt{2\bar{S}}\; a^\dagger\sqrt{1-\tfrac{a^\dagger a}{2\bar{S}}} \simeq \hbar\sqrt{2\bar{S}}\; a^\dagger; \\ \bar{S}_z &= \hbar\left(\bar{S} - a^\dagger a\right). \end{aligned} \tag{2.28}$$

So, by combining Eq. 2.27 and Eq. 2.28, we can write:

$$\begin{aligned} \bar{S}_x &= \tfrac{\sqrt{2\bar{S}}\hbar}{2}\left(a + a^\dagger\right); \\ \bar{S}_y &= \tfrac{\sqrt{2\bar{S}}\hbar}{2i}\left(a - a^\dagger\right); \\ \bar{S}_z &= \hbar\left(\bar{S} - a^\dagger a\right). \end{aligned} \tag{2.29}$$

Hence, the final form of the Hamiltonian in Eq. 2.30 is obtained after some lengthy calculations (contribution from P. van Dieten), where Eq. 2.29 is substituted in Eq. 2.23 to get to the final form of the Hamiltonian (Eq. 2.30), which reads:

$$H = \sum_{\langle ij \rangle} [t_{ij} a_i^\dagger a_j + t_{ij}^* a_i a_j^\dagger + \tau_{ij} a_i^\dagger a_j^\dagger + \tau_{ij}^* a_i a_j] + \sum_i [m_i a_i^\dagger a_i + m_i^* a_i a_i^\dagger + \mu_i a_i^\dagger a_i^\dagger + \mu_i^* a_i a_i] + E_0, \tag{2.30}$$

where t_{ij}, τij, m_i and μ_i are given by:

$$\begin{aligned}
t_{ij} &= \frac{\sqrt{S_i S_j}}{4} [D_\gamma^{ij} \left(G_{ij}^{\gamma xx} + G_{ij}^{\gamma yy} - i G_{ij}^{\gamma xy} + i G_{ij}^{\gamma yx} \right) - J \left(F_{ij}^{xx} + F_{ij}^{yy} - i F_{ij}^{xy} + i F_{ij}^{yx} \right)]; \\
\tau_{ij} &= \frac{\sqrt{S_i S_j}}{4} [D_\gamma^{ij} \left(G_{ij}^{\gamma xx} - G_{ij}^{\gamma yy} + i G_{ij}^{\gamma xy} + i G_{ij}^{\gamma yx} \right) - J \left(F_{ij}^{xx} - F_{ij}^{yy} + i F_{ij}^{xy} + i F_{ij}^{yx} \right)]; \\
m_i &= \frac{1}{2} K S_i \left(G_i^{zx} G_i^{zx} + G_i^{zy} G_i^{zy} \right) + \frac{1}{2} \lambda_i; \\
\mu_i &= \frac{1}{2} K S_i \left(G_i^{zx} G_i^{zx} - G_i^{zy} G_i^{zy} + i G_i^{zx} G_i^{zy} - i G_i^{zy} G_i^{zx} \right); \\
\lambda_i &= \sum_{j \in \{n_i\}} J S_j F_{ij}^{zz} - \sum_{j \in \{n_i\}} D_\gamma^{ij} S_j G_{ij}^{\gamma zz} - 2 K S_i G_i^{zz} G_i^{zz} + B G_i^{zz}.
\end{aligned} \tag{2.31}$$

Here n_i corresponds to the neighbours of each lattice site i. For instance, lattice site 25 has four direct neighbours; 24, 26, 41 and 9 from the left, right above and below respectively (see Fig. 2.1). Hence the sum over j in the λ_i term of Eq. (2.31) runs over all neighbours

2.5 Diagonalisation of the Hamiltonian

The Hamiltonian 2.30, with its parameters given from Eq. 2.31, is a bosonic system, the operators of which obey the well known commutation relations.

$$\begin{aligned}
\left[a_i, a_j^\dagger \right] &= \delta_{ij}; \\
[a_i, a_j] &= 0; \\
\left[a_i^\dagger, a_j^\dagger \right] &= 0.
\end{aligned} \tag{2.32}$$

Although the method of diagonalisation of such Hamiltonian is not trivial, it gives us useful information. A short review of the method is going to be discussed, following Xiao *et al.* [28] as well as Van Hemmen *et al.* [29].

The general form of a quadratic bosonic Hamiltonian reads:

$$H = \sum_{i,j} \alpha_{ij} c_i^\dagger c_j + \frac{1}{2}\gamma_{ij} c_i^\dagger c_j^\dagger + \frac{1}{2}\gamma_{ij}^* c_i c_j. \tag{2.33}$$

Eq. 2.33 can be more compactly written as:

$$H = \frac{1}{2}\psi^\dagger M \psi - \frac{1}{2} tr\left(\alpha\right), \tag{2.34}$$

where ψ, $\psi^\dagger$ and M are given by:

$$\psi = \begin{pmatrix} c \\ \tilde{c^\dagger} \end{pmatrix}; \qquad \psi^\dagger = \begin{pmatrix} c^\dagger & \tilde{c} \end{pmatrix}; \qquad M = \begin{pmatrix} \alpha & \gamma \\ \gamma^\dagger & \tilde{\alpha} \end{pmatrix}, \tag{2.35}$$

where $\tilde{c}$ is the transpose of c and it is given by:

$$c = \begin{pmatrix} c_1 \\ c_2 \\ \vdots \\ c_n \end{pmatrix}; \qquad c^\dagger = \begin{pmatrix} c_1^\dagger & c_2^\dagger & \dots & c_n^\dagger \end{pmatrix}. \tag{2.36}$$

Let us for simplicity define

$$c_i \cdot c_j = \left[c_i, c_j\right], \tag{2.37}$$

that allows us to rewrite the bosonic commutation relations (2.32) as:

$$\psi \cdot \psi^\dagger = I_-, \tag{2.38}$$

with I_- to be defined as:

$$I_- = \begin{pmatrix} I & 0 \\ 0 & -I \end{pmatrix}. \tag{2.39}$$

The Bogoliubov-Valatin transformation is then performed by

$$c = Ad + B\tilde{d^\dagger}, \tag{2.40}$$

where d is given as:

$$d = \begin{pmatrix} d_1 \\ d_2 \\ \vdots \\ d_n \end{pmatrix}; \qquad d^\dagger = \begin{pmatrix} d_1^\dagger & d_2^\dagger & \dots & d_n^\dagger \end{pmatrix}. \tag{2.41}$$

This gives rise to:

$$\phi \cdot \phi^\dagger = I_-, \tag{2.42}$$

with:

$$\phi = \begin{pmatrix} d \\ \tilde{d}^\dagger \end{pmatrix}; \qquad \phi^\dagger = \begin{pmatrix} d^\dagger & \tilde{d} \end{pmatrix}. \tag{2.43}$$

Combining Eq. 2.36, 2.40 and 2.41, we can find

$$\psi = T\phi; \qquad T = \begin{pmatrix} A & B \\ B^* & A^* \end{pmatrix}. \tag{2.44}$$

Then, the Hamiltonian can be written as:

$$H = \frac{1}{2}\phi^\dagger T^\dagger M T \phi - \frac{1}{2} tr\left(\alpha\right), \tag{2.45}$$

and Eq. 2.38 is now written as:

$$T I_- T^\dagger = I_-. \tag{2.46}$$

For the Hamiltonian 2.45 to be diagonal, it is necessary for $T^\dagger M T$ to be diagonal.

$$T^\dagger M T = \begin{pmatrix} \omega_1 & 0 & 0 & \cdots & 0 \\ 0 & \omega_2 & 0 & \cdots & 0 \\ \vdots & \vdots & \vdots & \ddots & \vdots \\ 0 & 0 & 0 & \cdots & \omega_{2n} \end{pmatrix}. \tag{2.47}$$

So under these conditions we have:

$$H = \frac{1}{2}\sum_{i=1}^{n}\left(\omega_i - \omega_{n+i}\right) d_i^{\dagger} d_i + \frac{1}{2}\sum_{i=1}^{n}\omega_{n+i} - \frac{1}{2} tr\left(\alpha\right). \tag{2.48}$$

This is the so-called diagonal form of the Hamiltonian 2.33, with $d_i^{\dagger}$ and d_i bosonic operators. The interested reader can read more about the diagonalisation procedure [29], [28] and [30].

2.6 The Hall Conductivity

In this chapter we find the relation that describes the thermal Hall effect of magnons in terms of quantities that we can numerically compute.

In section 1.1 the Hall effect of charged particles was discussed and the transverse conductivity was found to be given from Eq. 1.6. However, this equation cannot be used to describe the thermal Hall effect of magnons because:

1. It strictly depends on the charge of the particles and as we have seen magnons are neutral quasiparticles.

2. It requires the presence of a Lorentz type magnetic force which is absent in the thermal Hall effect of magnons.

Matsumoto *et al.* [31] have proven a formula which relates the transverse thermal conductivity for neutral particles (or quasiparticles) with quantities that can be computed. This formula reads:

$$\kappa_{xy} = -\frac{k_B^2 T}{\hbar V}\sum_{n,k} c_2\left(\rho_n\right)\Omega_{n,z}\left(k\right). \tag{2.49}$$

To make things worse, this equation cannot be used since our ground states are skyrmionic and the magnon Hamiltonian is not diagonalised by means of Fourier transform because the presence of the skyrmion lattice breaks translation symmetry .

As discussed in section 2.2 the Hamiltonian of the system consists of four different terms (exchange interactions, DM interaction, anisotropy term and external magnetic field). The presence of the DMI is fruitful because it makes the system lack inversion symmetry and it leads to the creation of chiral magnons with nontrivial topological

properties [11]. Furthermore, the presence of the DMI generates configurations with non vanishing Berry curvature, which acts as an effective magnetic field [7] (Eq. 1.20), that magnons can feel, giving rise to the thermal Hall effect.

Therefore, the thermal conductivity will firstly depend on Berry curvature (i.e. the effective magnetic field) and secondly on the number of magnons excited. It has to be mentioned that a strict mathematical formula for the Hall conductivity requires techniques that are beyond the level of the Thesis hence we are only interested in the trend of the the thermal conductivity.

After stating these rules, we are ready to give the simplest mathematical relation which connects the transverse thermal conductivity with the number of magnons and the effective magnetic field and it reads:

$$\kappa_{xy} \propto n_m B^{eff}, \tag{2.50}$$

where n_m is the number of magnons and B^{eff} the effective magnetic field.

Below, we present the method followed to obtain these two quantities. The number of magnons is discussed in 2.6.1, subsequently, two ways to compute the effective magnetic field are intrduced. The first one in section 2.6.2 while the latter one in section 2.6.3.

2.6.1 Number of Magnons

In section 2.5 we showed that magnons are bosons, since their operators obey the standard commutation relations. This is extremely important because it allows us to compute the average number of some bosons at each state using Bose-Einstein statistics. The relation which gives us the average number is given by:

$$\rho_i\left(\epsilon_i\right) = \frac{1}{e^{\beta\epsilon_i} - 1}. \tag{2.51}$$

where ρ_i stands for the average, i runs over all possible energy states of the system, $\beta = \frac{1}{k_B T}$ the inverse temperature with k_B the Boltzmann constant and ϵ_i the energy of each level. It can be easily understood that the total number of particles N of a system which consists of r energy levels will be the sum of the average number of

particles at all levels:

$$N = \sum_{i=0}^{r} \rho_i(\epsilon_i) = \sum_{i=0}^{r} \frac{1}{e^{\beta\epsilon_i} - 1}. \tag{2.52}$$

Regarding magnon number we have to compute, the procedure is similar but more complicated. First of all, in section 2.5 the eigenvalues ω_i of the Hamiltonian were computed. Since the method is based on doubling the Hamiltonian of the system, we are only interested in half of the eigenvalues, the ones that correspond to positive values, due to the positive definiteness of the matrix. This means that the eigenvalues ω_i are sorted in ascending order, which are labeled as $\bar{\omega}_i$. Furthermore, the different cases (ferromagnets and antiferromagnets) differ in the number of modes as well because the first mode of the antiferromagnetic lattice corresponds to translation motion of lattice and therefore it is neglected. In order to be able to write a general formula for both cases, we have to introduce a new symbol, inspired from Kronecker's delta. This symbol is defined as:

$$\delta_{c,AFM} = \begin{cases} 1, & \text{if} \quad c = \text{AFM} \\ 0, & \text{if} \quad c \neq \text{AFM}. \end{cases} \tag{2.53}$$

Similarly, we can define:

$$\delta_{c,FM} = \begin{cases} 1, & \text{if} \quad c = \text{FM} \\ 0, & \text{if} \quad c \neq \text{FM}. \end{cases} \tag{2.54}$$

As it is obvious $c \in \{\text{FM}, \text{AFM}\}$.

Therefore, using Eq. 2.52 we can write:

$$n_{m,c} = \sum_{a=L_{x,c}L_{y,c}+1+\delta_{c,AFM}}^{2L_{x,c}L_{y,c}} \frac{1}{e^{\beta\hbar\bar{\omega}_{\alpha,c}} - 1}, \tag{2.55}$$

with $n_{m,c}$ to be the total number of magnons of our system. The index α runs from $L_{x,c}L_{y,c} + 1 + \delta_{c,AFM}$ up to $2L_{x,c}L_{y,c}$ because we are interested in the second half of the eigenvalues.

2.6.2 Effective Magnetic Field

Next, the procedure to find the effective magnetic field B^{eff} is discussed.

The Hamiltonian of the system (Eq. 2.30) can be written as:

$$H = \sum_{i,j=1}^{m} \begin{pmatrix} a_i^\dagger & a_j \end{pmatrix} \begin{pmatrix} H_{ij} \end{pmatrix} \begin{pmatrix} a_j \\ a_i^\dagger \end{pmatrix}. \tag{2.56}$$

The method of diagonilisation (analysed in section 2.5) implies that the Hamiltonian matrix H_{ij} is written as:

$$(H_{ij}) = \begin{pmatrix} \boxed{A} & \boxed{B} \\ \boxed{B^*} & \boxed{A^*} \end{pmatrix};$$

with A and B sub-matrices responsible for the $a_i^\dagger a_j$ (and $a_i a_j^\dagger$) and $a_i a_j$ (and $a_i^\dagger a_j^\dagger$) part of the Hamiltonian respectively.

From now on, we only focus on the top left part of the Hamiltonian matrix H_{ij} [32], which is for simplicity denoted by A_{ij} and it is the matrix containing the hopping amplitudes. Henceforth, the Hamiltonian is approximated as:

$$H_{ij} \approx A_{ij}. \tag{2.57}$$

Considering this approximation and the so called Peierls substitution:

$$t_{ij} \to t_{ij} e^{ie \int_i^j \mathbf{A} dr}, \tag{2.58}$$

where the integral in the exponent is the phase a particle acquires while moving from the point "i" of the lattice to the adjacent point "j" [33], we write the Hamiltonian matrix as [34, 35]:

$$H_{ij} = A_{ij} e^{i\phi_{ij}}. \tag{2.59}$$

In order to eliminate the tunneling amplitude A_{ij}, we write separately the real and the imaginary part of Eq. 2.59.

$$\begin{aligned} \mathrm{Re}(H_{ij}) &= A_{ij} \cos\phi_{ij}; \\ \mathrm{Im}(H_{ij}) &= A_{ij} \sin\phi_{ij}. \end{aligned} \tag{2.60}$$

After solving for ϕ_{ij} we obtain:

$$\phi_{ij} = \arctan\left(\frac{\mathrm{Im}(H_{ij})}{\mathrm{Re}(H_{ij})}\right). \tag{2.61}$$

It is important to realise that ϕ_{ij} are the phases of the hopping amplitudes and they live on the links between the two neighbouring spins.

In order to compute the magnetic field, we should first define the magnetic flux as:

$$\Phi_B = \iint_S \mathbf{B} \cdot d\mathbf{S}, \tag{2.62}$$

which is the magnetic flux that passes through an area S with magnetic field B.

Fig. 2.6 illustrates the magnetic flux passing through a circular area A (left part) and a magnetic flux passing through a plaquette of area A of a lattice (right).

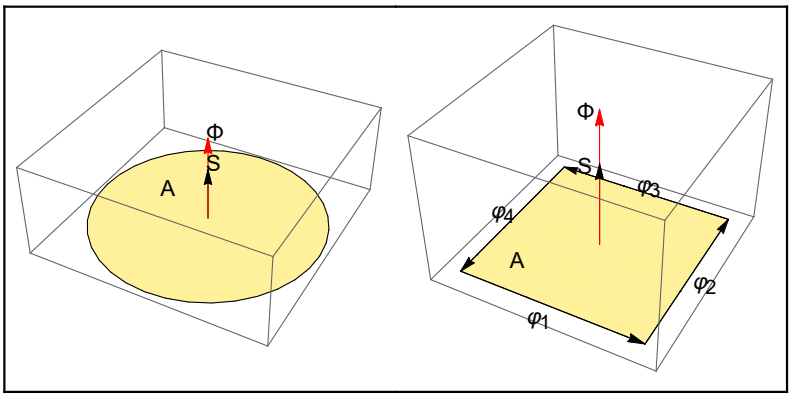

Figure 2.6: Magnetic field of a lattice's plaquette.

By assuming that the magnetic field points to the z-direction, it can be proven that [36]:

$$\Phi_{B,i} \approx b_i, \tag{2.63}$$

where $\Phi_{B,i}$ is the magnetic flux through each plaquette i and b_i the effective magnetic field at each plaquette i.

It is clear now that by computing the magnetic flux through each plaquette of the lattice, we are able to estimate the effective magnetic field.

- **A toy model:**

In order to make the procedure of finding the effective magnetic field easier, we will first consider a 3×3 lattice toy model and explicitly compute the magnetic flux (magnetic field) over its plaquettes. The effective magnetic fields of our ground states are then computed in the same way.

Fig. 2.7 and Eq. 2.66 show everything we need to know for the toy model. The matrix ϕ of Eq. 2.66 can be computed from the Hamiltonian matrix by using Eq. 2.61. This is a 9×9 matrix because there are 9 spins in the configuration. Since only nearest neighbouring interaction were taken into account, all of the other elements (except the diagonals) are zero. Regarding the diagonal elements, they correspond to the probability of the particles to stay at the same position and therefore they are not used in this part of the Thesis. All of the terms that are either zero or not-used, have been crossed out from the matrix by a red line. The remaining terms are enclosed in a coloured box, the importance of which is discussed.

In Fig. 2.7, the blue dots represent the position of the spin vectors on the lattice and the red numbers stand for numbering them. The remaining elements of the matrix in Eq. 2.66 correspond to phase of the hopping between two neighbouring spins and they are demarcated as black arrows in Fig. 2.7. Green labels match the visible black arrows with the appropriate matrix element ϕ_{ij}, where the convention $\phi_{i\to j} = \phi_{ji}$ has been used. Four specific black arrows close a loop among four spins. All of these loops are numbered by the black numbers visible in Fig. 2.7.

Below, we explicitly compute the magnetic flux at each of the six loops visible in Fig. 2.7. The expressions follow:

$$\begin{aligned}
\Phi_1 &= \phi_{1\to 2} + \phi_{2\to 5} + \phi_{5\to 4} + \phi_{4\to 1};\\
\Phi_2 &= \phi_{2\to 3} + \phi_{3\to 6} + \phi_{6\to 5} + \phi_{5\to 2};\\
\Phi_3 &= \phi_{4\to 5} + \phi_{5\to 8} + \phi_{8\to 7} + \phi_{7\to 4};\\
\Phi_4 &= \phi_{5\to 6} + \phi_{6\to 9} + \phi_{9\to 8} + \phi_{8\to 5};\\
\Phi_5 &= \phi_{3\to 1} + \phi_{1\to 4} + \phi_{4\to 6} + \phi_{6\to 3};\\
\Phi_6 &= \phi_{6\to 4} + \phi_{4\to 7} + \phi_{7\to 9} + \phi_{9\to 6}.
\end{aligned} \tag{2.64}$$

The sum of the magnetic fluxes at each plaquette will give us the total effective magnetic field of the configuration, as the next formula indicates:

$$B^{eff} \approx \frac{1}{2\pi} \sum_{i=1}^{6} \Phi_i. \tag{2.65}$$

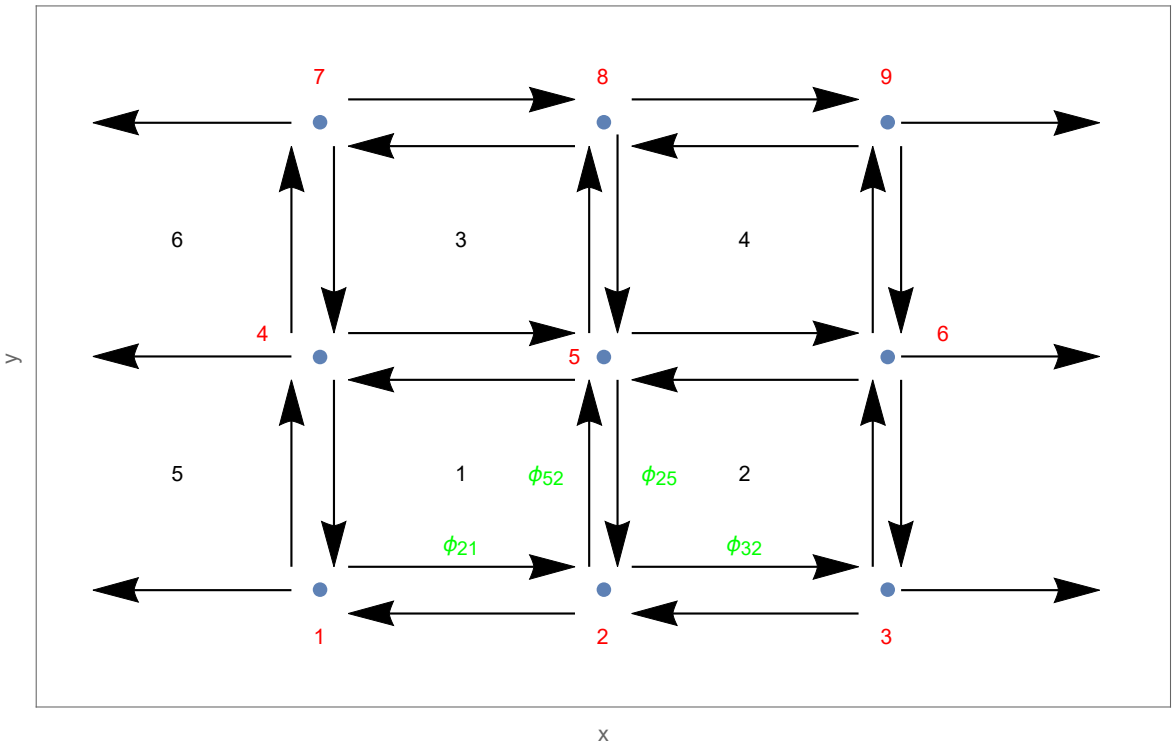

Figure 2.7: Draft configuration.

$$\phi = \begin{pmatrix} \phi_{1\to1} & \phi_{1\to2} & \phi_{1\to3} & \phi_{1\to4} & \phi_{1\to5} & \phi_{1\to6} & \phi_{1\to7} & \phi_{1\to8} & \phi_{1\to9} \\ \phi_{2\to1} & \phi_{2\to2} & \phi_{2\to3} & \phi_{2\to4} & \phi_{2\to5} & \phi_{2\to6} & \phi_{2\to7} & \phi_{2\to8} & \phi_{2\to9} \\ \phi_{3\to1} & \phi_{3\to2} & \phi_{3\to3} & \phi_{3\to4} & \phi_{3\to5} & \phi_{3\to6} & \phi_{3\to7} & \phi_{3\to8} & \phi_{3\to9} \\ \phi_{4\to1} & \phi_{4\to2} & \phi_{4\to3} & \phi_{4\to4} & \phi_{4\to5} & \phi_{4\to6} & \phi_{4\to7} & \phi_{4\to8} & \phi_{4\to9} \\ \phi_{5\to1} & \phi_{5\to2} & \phi_{5\to3} & \phi_{5\to4} & \phi_{5\to5} & \phi_{5\to6} & \phi_{5\to7} & \phi_{5\to8} & \phi_{5\to9} \\ \phi_{6\to1} & \phi_{6\to2} & \phi_{6\to3} & \phi_{6\to4} & \phi_{6\to5} & \phi_{6\to6} & \phi_{6\to7} & \phi_{6\to8} & \phi_{6\to9} \\ \phi_{7\to1} & \phi_{7\to2} & \phi_{7\to3} & \phi_{7\to4} & \phi_{7\to5} & \phi_{7\to6} & \phi_{7\to7} & \phi_{7\to8} & \phi_{7\to9} \\ \phi_{8\to1} & \phi_{8\to2} & \phi_{8\to3} & \phi_{8\to4} & \phi_{8\to5} & \phi_{8\to6} & \phi_{8\to7} & \phi_{8\to8} & \phi_{8\to9} \\ \phi_{9\to1} & \phi_{9\to2} & \phi_{9\to3} & \phi_{9\to4} & \phi_{9\to5} & \phi_{9\to6} & \phi_{9\to7} & \phi_{9\to8} & \phi_{9\to9} \end{pmatrix} \tag{2.66}$$

- **The general case:**

The toy model consists of 6 loops and therefore it is easy to explicitly compute every term. The ground states though consist of more loops, which practically makes listing of the magnetic fluxes impossible. This problem can be solved by compactly writing all magnetic fluxes in one equation. This is not the end of the story though since ferromagnetic and antiferromagnetic configurations differ in the number of boundary conditions, hence the symbols $\delta_{c,AFM}$ and $\delta_{a,FM}$ which were introduced in the previous subsection and more specifically from Eq. 2.53 and Eq. 2.54 respectively, have to be used. As a consequence, the index "i" has to bound itself at the number $L_x\,(L_y - \delta_{c,FM})$. After considering these restrictions, we end up with the following expression [33][1]:

$$\Phi_{i,c} = \begin{cases} \phi_{i\to i+1} + \phi_{i+1\to i+1+L_x} + \phi_{i+1+L_x\to i+Lx} + \phi_{i+Lx\to i} & \text{if} \quad i \neq nL_x \\ \phi_{i\to i+1-L_x} + \phi_{i+1-L_x\to i+1} + \phi_{i+1\to i+Lx} + \phi_{i+Lx\to i} & \text{if} \quad i = nL_x; \end{cases} \tag{2.67}$$

with $i \in \{x \mid x \in \mathbb{N}^+ \mid x < L_x L_y\}$ due to the boundary conditions,
$n \in \{x \mid x \in \mathbb{N}^+ \mid x < (L_y - \delta_{c,FM})\}$ and ϕ_{jk} to be the elements of the matrix in Eq. 2.66.

Finally, the effective magnetic field will be given by the sum of the magnetic fluxes, as Eq. 2.65 indicates. Hence, the compact form is written as:

$$B_c^{eff} \approx \frac{1}{2\pi} \sum_{i=1}^{L_{x,c}\left(L_{y,c}-\delta_{c,FM}\right)} \Phi_{i,c}. \tag{2.68}$$

2.6.3 Adiabatic Approximation

Alternatively, the adiabatic approximation provides us another way to extract the effective magnetic filed of our lattices.

The basic idea is to map the existing problem, which is a magnon traversing a spatially magnetic texture with constant amplitude, onto a problem, where the magnon moves in a uniform Zeeman magnetic field, but instead feels an additional

[1] In [33] the expression for the total flux (at position (m,n)) reads: $\Phi_{m,n} = \phi^x_{m,n} + \phi^y_{m+1,n} - \phi^x_{m,n+1} - \phi^y_{m,n}$. The difference in the last two minus signs comes from the way the matrix elements are computed and the orientation of their vectors. The two formulas are equivalent.

emergent electric and magnetic field [7]. The expression for the magnetic field is given by:

$$\mathbf{b}_i^e = \frac{\hbar}{2}\epsilon_{i,j,k}\hat{\mathbf{M}}\cdot\left(\partial_j\hat{\mathbf{M}}\times\partial_k\hat{\mathbf{M}}\right), \tag{2.69}$$

where $\hat{\mathbf{M}} = \mathbf{M}/M$ the local magnetisation direction. The interested reader can find more information regarding the derivation of this formula in the suggested literature [7].

Since we are only interested in the z-direction of the emergent magnetic field, we can plug $i = z$ in Eq. 2.69 and after some simple algebra, we have:

$$b_z^e = \hbar\hat{\mathbf{M}}\cdot\left(\partial_x\hat{\mathbf{M}}\times\partial_y\hat{\mathbf{M}}\right). \tag{2.70}$$

The interested reader can find more information in the following articles: [7, 37] and [38, 39].

In order to find an expression that can be used to give us the emergent magnetic field of our lattice, we have to perform some algebraic manipulations to Eq. 2.70. Expanding the cross product by using the rule

$$\mathbf{a}\times\mathbf{b} = \begin{pmatrix} \mathbf{x} & \mathbf{y} & \mathbf{z} \\ a_x & a_y & a_z \\ b_x & b_y & b_z \end{pmatrix}; \tag{2.71}$$

allows us to write Eq. 2.69 as:

$$\begin{aligned} b_z^e = &\left(\frac{\partial M_y}{\partial x}\frac{\partial M_z}{\partial y} - \frac{\partial M_y}{\partial y}\frac{\partial M_z}{\partial x}\right)M_x \\ &- \left(\frac{\partial M_x}{\partial x}\frac{\partial M_z}{\partial y} - \frac{\partial M_x}{\partial y}\frac{\partial M_z}{\partial x}\right)M_y \\ &+ \left(\frac{\partial M_y}{\partial x}\frac{\partial M_x}{\partial y} - \frac{\partial M_x}{\partial y}\frac{\partial M_y}{\partial x}\right)M_z. \end{aligned} \tag{2.72}$$

Eq. 2.72 has to be discretised in order to be used for our lattice. This can be done by simply changing the derivatives with the difference of the magnetisation vectors at the underlined direction. In such way we have:

$$
\begin{aligned}
b^e_{i,c} = &\left[\left(M^y_r - M^y_i\right)\left(M^z_u - M^z_i\right) - \left(M^y_u - M^y_i\right)\left(M^z_r - M^z_i\right)\right] M^x_i \\
&- \left[\left(M^x_r - M^x_i\right)\left(M^z_u - M^z_i\right) - \left(M^x_u - M^x_i\right)\left(M^z_r - M^z_i\right)\right] M^y_i \\
&+ \left[\left(M^x_r - M^x_i\right)\left(M^y_u - M^y_i\right) - \left(M^x_u - M^x_i\right)\left(M^y_r - M^y_i\right)\right] M^z_i;
\end{aligned} \tag{2.73}
$$

where $i \in \{1, L_x L_y\}$ and stands for the lattice points. r and u are the right and the upper neighbour of i respectively. Finally, x, y, z stand for the Cartesian coordinates of the magnetisation vector.

2.6.4 Final Expression

We have already seen that the transverse conductivity is given by Eq. 2.50 and that the two terms that it consists of can be written, in terms of the parameters of the configuration, as given by Eq. 2.55 and Eq. 2.68 respectively. In this subsection we form the final expression for the transverse thermal conductivity into a single, compact formula.

$$
\kappa_{xy,c} \propto \sum_{\alpha = L_{x,c}L_{y,c}+1+\delta_{c,AFM}}^{2L_{x,c}L_{y,c}} \sum_{i=1}^{L_{x,c}\left(L_{y,c}-\delta_{c,FM}\right)} \left(\frac{1}{e^{\beta\hbar\bar{\omega}_{\alpha,c}} - 1}\right) b_{i,c}. \tag{2.74}
$$

Alternatively, we can use Eq. 2.73 instead of Eq. 2.67.

Table 2.3 summarises the symbols in Eq. 2.74.

Symbol	Stands for the...	Value
c	Index to distinguish the two different cases	$c \in \{\text{FM}, \text{AFM}\}$
$\delta_{c,FM}, \delta_{c,AFM}$	Kronecker's delta of the configurations	Eq, 2.54 and Eq. 2.53
$L_{x,FM}$	Length of the ferromagnetic configuration	16
$L_{y,FM}$	Width of the ferromagnetic configuration	16
$L_{x,AFM}$	Length of the antiferromagnetic configuration	32
$L_{y,AFM}$	Width of the antiferromagnetic configuration	32
$\bar{\omega}_{\alpha,c}$	Sorted eigenvalues of the Hamiltonian	Numerical simulation
$b_{i,c}$	Magnetic field at a specific closed loop	Eq. 2.67 or Eq. 2.73

Table 2.3: Explanation of symbols present in Eq. 2.74.

Eq. 2.74 is all we need in order to compute the thermal transverse conductivity $\kappa_{xy,c}$.

CHAPTER 3

Results

In the present Chapter, we present the result found using the theory and the methodology discussed in Chapter 2. The figures were created using Mathematica 10 [40] as well as "TikZ" and the numerical procedure by using both a self-constructed C++ code and the "Armadillo C++" external library [41]. The section is divided in three subsections. The first one deals with ferromagnets and the second one with antiferromagnets. Finally the third subsection compares the result of the previous two. In the rest of this chapter "a" is the lattice constant and it is used to make quantities dimensionless and $\hbar = 1$.

3.1 Ferromagnets

The ground state is a 16×16 skyrmionic lattice visible in Fig. 2.2. Below, we present the dispersion of the system, the average magnon occupation per energy state, the effective magnetic field distribution and some possible comparisons that can be done by altering specific parameters. The mosaic of the chapter is completed by showing the thermal dependency of the transverse conductivity.

3.1.1 Dispersion

In Fig. 3.1 the dispersion of the ground state of Hamiltonian 2.17 is depicted (the coupling constants are in Table 2.1). To compare, we can see, in the appendix, the dispersion of the Hamiltonian B.1 with ferromagnetic coupling $J > 0$ in the left part of Fig. B.1.

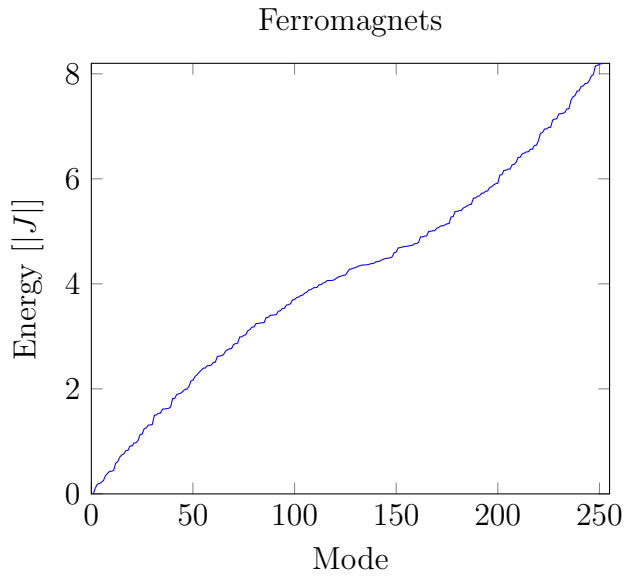

Figure 3.1: Dispersion of the system (ferromagnets).

3.1.2 Magnon Occupation

Since magnons are bosons, they will obey to the Bose-Einstein statistics (Eq. 2.51). In Fig. 3.2 the average number of magnons in each state is depicted. Different colours correspond to different values of β. As temperature decreases (β increases) less states are occupied.

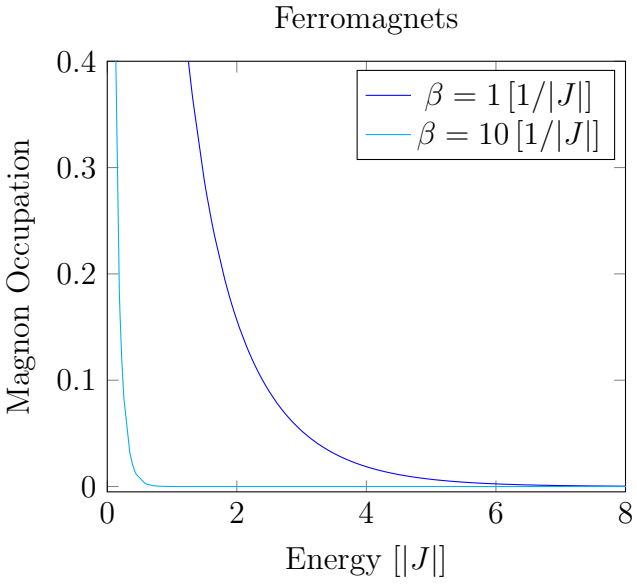

Figure 3.2: Occupation of magnons at each state (ferromagnets).

3.1.3 Effective Magnetic Field

In subsection 2.6 we discussed the equivalence of the Berry curvature and the effective magnetic field. Subsequently, in subsections 2.6.2 and 2.6.3 two methods to

numerically compute the effective magnetic field were analysed. In this subsection we present the effective magnetic field found according to the previous analysis.

Fig. 3.3 illustrates the distribution of the effective magnetic field (or Berry curvature) computed with the method of section 2.6.2. If we compare the effective magnetic field distributions with the ground state in colour plot, as shown in Fig. 3.4, it becomes clear that the presence of the skyrmion gives rise to large values of the magnetic field.

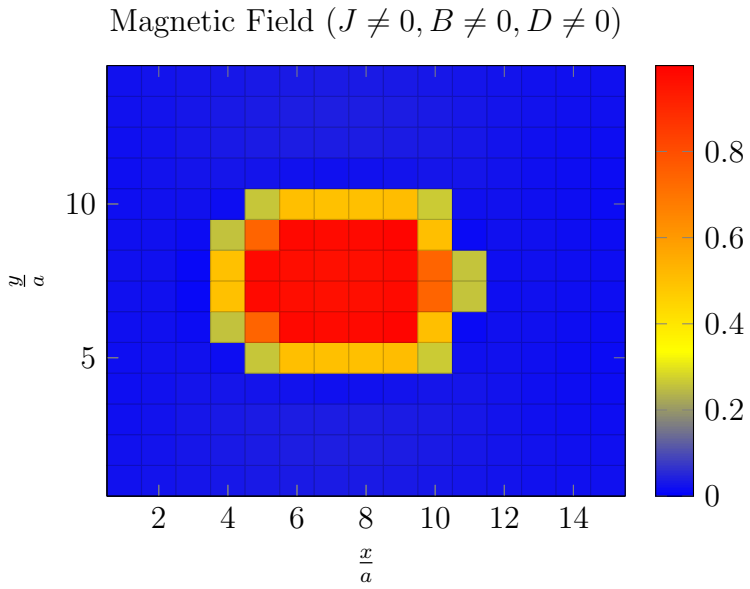

Figure 3.3: Magnetic field distribution using Eq. 2.67 (ferromagnets).

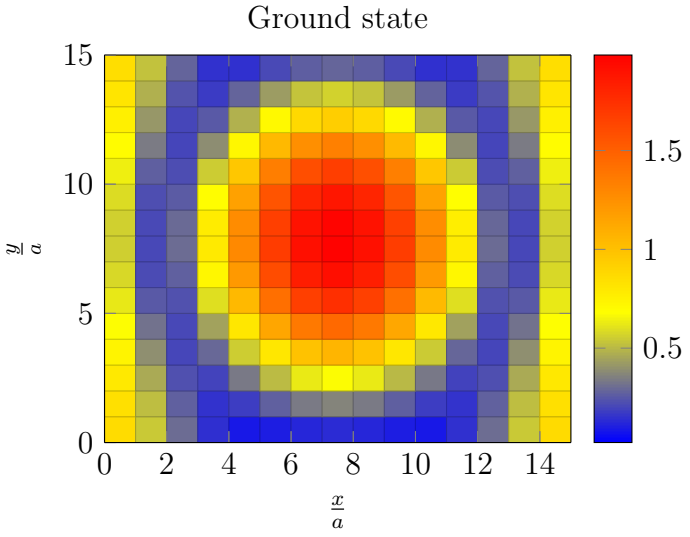

Figure 3.4: Colour plot of the ferromagnetic ground state.

We can also compute the effective magnetic field by using the adiabatic approximation of section 2.6.3. The result is shown in Fig. 3.5. Again, this result is comparable to

the colour plot of the ground state (Fig. 3.4).

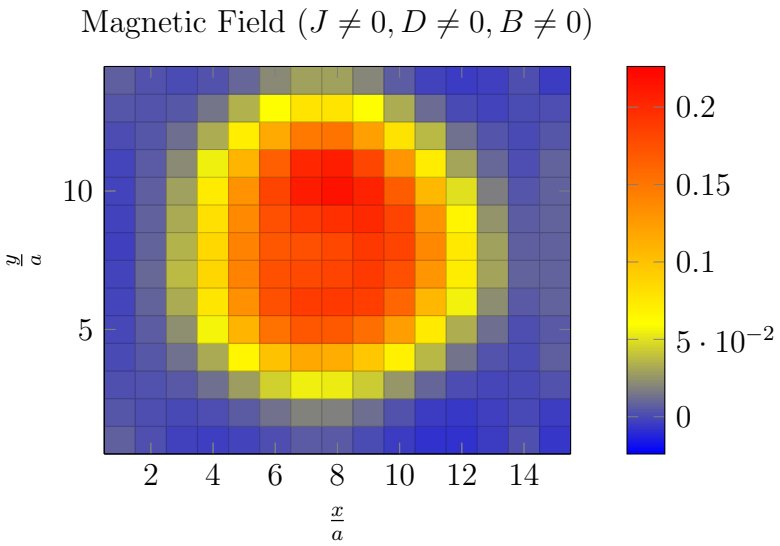

Figure 3.5: Magnetic field distribution using Eq. 2.73 (ferromagnets).

3.1.4 Comparisons

In this subsection, we theoretically investigate the behaviour of the effective magnetic field for different values of the coupling constants of the Hamiltonian 2.17.

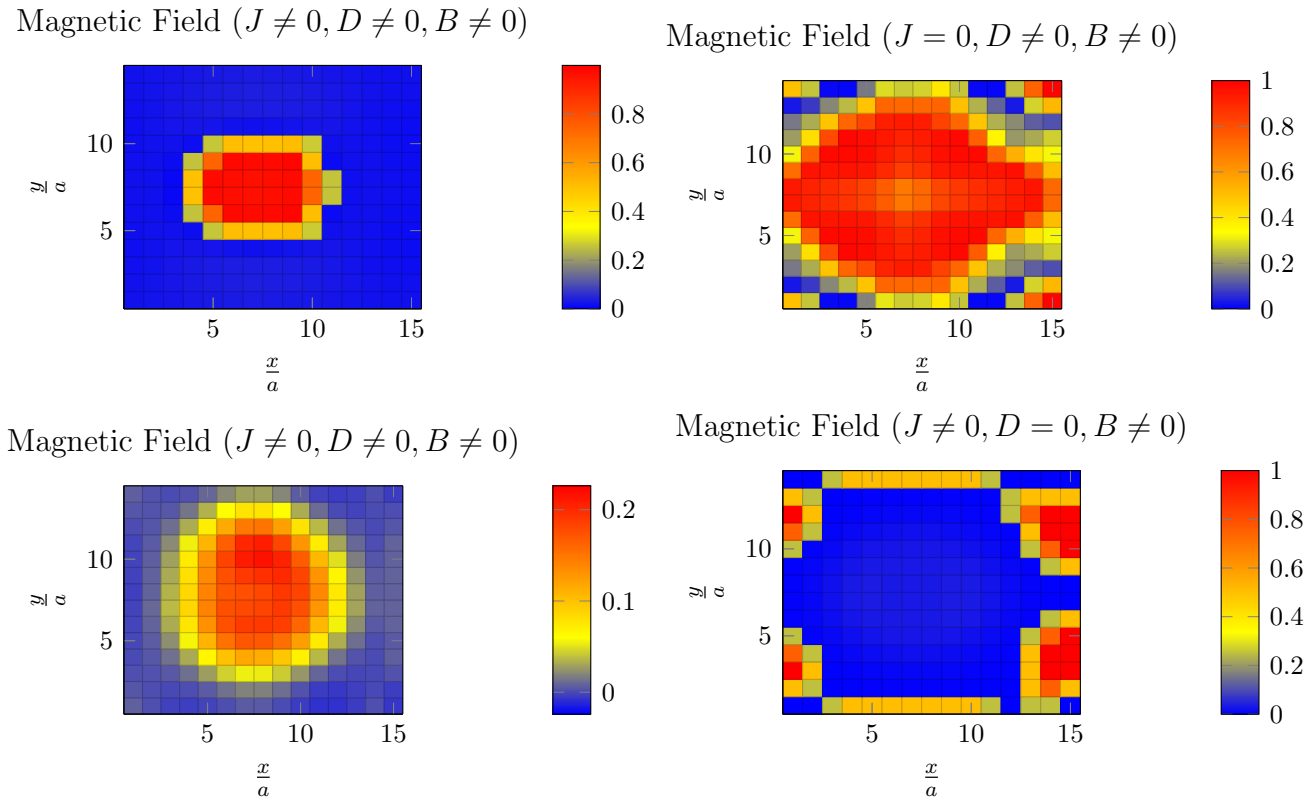

Figure 3.6: Distribution of the effective magnetic field for different values of Hamiltonian's coupling constants (ferromagnets).

In Fig. 3.6 the magnetic field distributions for different values of couplings of the Hamiltonian are illustrated. More specifically, the top left and the bottom left part of the graph correspond to the full results explained in the previous section (the top one was computed with the methodology discussed in section 2.6.2 and the bottom one with the methodology of section 2.6.3). The top right part of Fig. 3.6 shows how would the result of the magnetic field be, if there was no exchange interaction among spins ($J = 0$). Finally, the bottom right part shows the hypothetical magnetic field distribution of a Hamiltonian without Dzyaloshinskii-Moriya interaction ($D = 0$). As it is obvious, both figures on the right part have no similarities with the initial skyrmionic configuration, making them incorrect. This proves that the correct result of the magnetic field distribution is only computed by using the Hamiltonian which depends on all of the four terms described in section 2.2 and therefore only the left part of the Figure is correct.

An alternative way to represent the distribution of the magnetic field for $J \neq 0$, $D \neq 0$ and $B \neq 0$ in the Hamiltonian, is the one shown in Fig. 3.7. The height of each point corresponds to the value of the effective magnetic field and the colour just to make it easier recognisable.

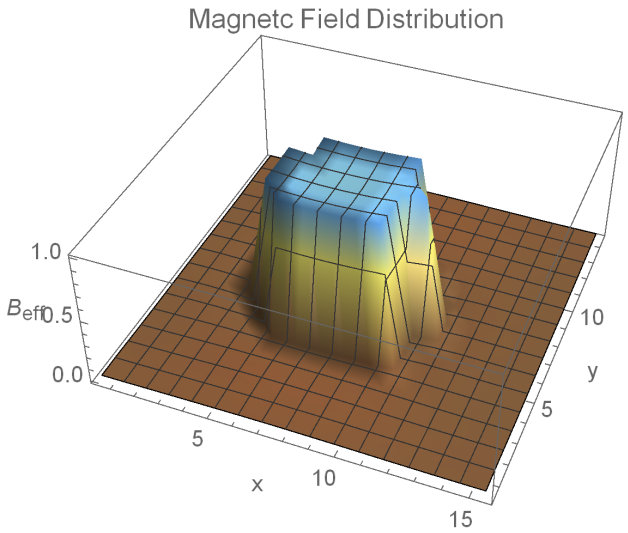

Figure 3.7: The effective magnetic field in three-dimensions using Eq. 2.67.

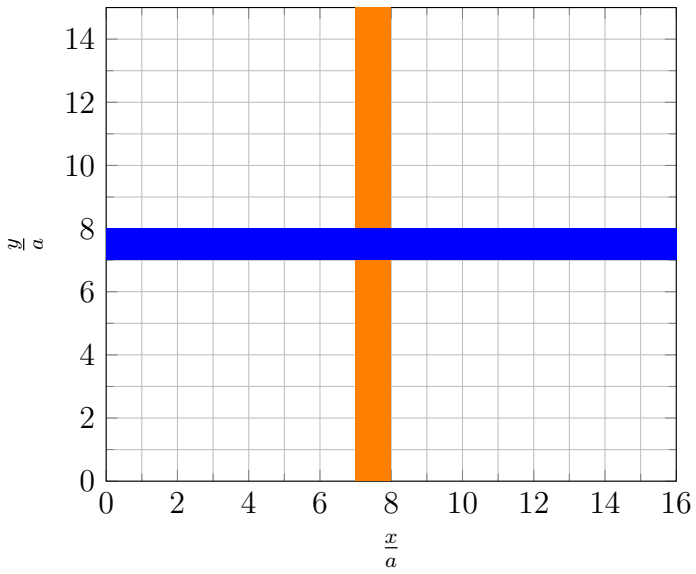

Figure 3.8: Lines along which the values of the effective magnetic field in Fig. 3.9 and Fig. 3.10 were taken.

Since the effective magnetic field computed with the formula in section 2.6.2 depicted in Fig. 3.7 is due to the skyrmion we can simply plot its values along a line in the middle of the lattice in both directions (see Fig. 3.8). More specifically, Fig. 3.9 and Fig. 3.10 illustrate the values of the effective magnetic field in x and y direction respectively for y and x fixed at 8 respectively (blue and orange in Fig. 3.8 respectively). The different colours correspond to different values of couplings in the Hamiltonian 2.17. From these figures, it is obvious that the correct contribution to the effective magnetic field in both directions depends on both J and D and if we switch one of these constants off, the result is not the desired one. Therefore only the red line represents the correct effective magnetic field.

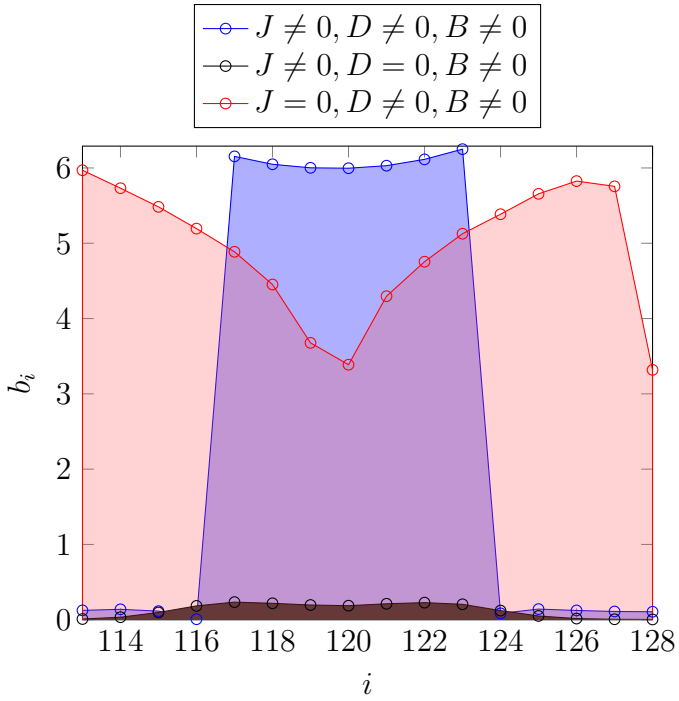

Figure 3.9: Values of the effective magnetic field along the x-axis ($y = 8$). In this case $113 \leq i \leq 128$

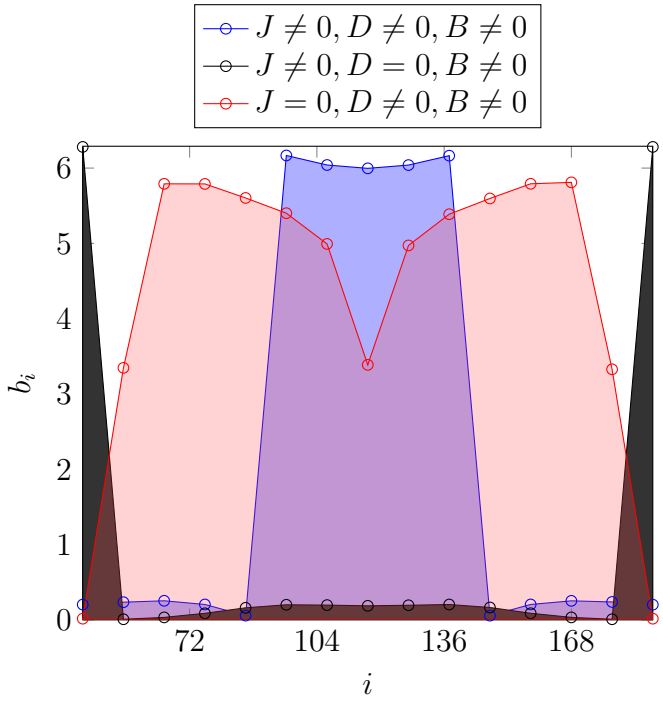

Figure 3.10: Values of the effective magnetic field along the y-axis ($x = 8$). In this case $i \in \{kL_x/2 \mid k \in \mathbb{N}^+ \mid k < L_x\}$

3.1.5 Hall Conductivity

By using Eq. 2.74 it is easy to compute the values of the thermal transverse conductivity for certain values of the inverse temperature β. However, temperature T, as a physical quantity, is better understood and therefore Fig. 3.11 illustrates the dependency of the transverse thermal conductivity on temperature. The blue colour stands for the transverse thermal conductivity computed using the method of section 2.6.2 (full result) whereas the light blue with the method discussed in section 2.6.3 (adiabatic approximation).

- For $T = 0$ there is no conductivity and therefore no Hall effect.
- For $T > 0$ we can see a linear behaviour for both cases[1].

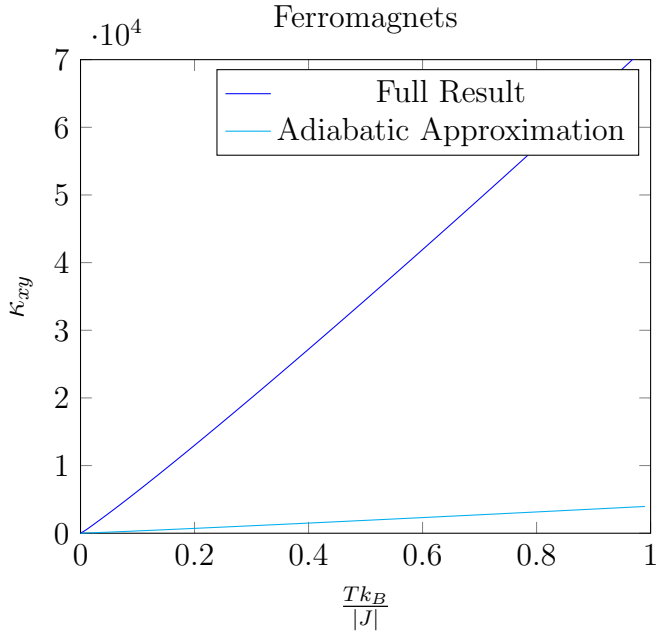

Figure 3.11: Transverse thermal conductivity as a function of temperature in ferromagnets computed with the two different methods.

[1] A quadratic fit of the form $a + bx + cx^2$ with a, b, c the unknown coefficients of the fit, will only improve R^2 in the 4th decimal place hence we can safely say that the data has linear behaviour. You can see R^2 values for the linear and the quadratic fit in the following table.

Fit	R^2
Linear	0.999849
Quadratic	0.999994

3.2 Antiferromagnets

In this case the ground state is a 32×32 skyrmionic lattice, visible in Fig. 2.4. Similarly to ferromagnets, the dispersion of the system, the average magnon occupation per energy state, the effective magnetic field distribution and its comparison with situations in which the exchange interaction and Dzyaloshinskii-Motriya interaction vanish are discussed. Finally the thermal dependency of the transverse conductivity is shown.

3.2.1 Dispersion

In Fig. 3.12 the dispersion of the ground state of the Hamiltonian 2.17 is depicted (the coupling constants are visible in Table 2.2). To compare, we can see, in the appendix, the dispersion of the Hamiltonian B.1 with antiferromagnetic coupling $J < 0$ in the right part of Fig. B.1.

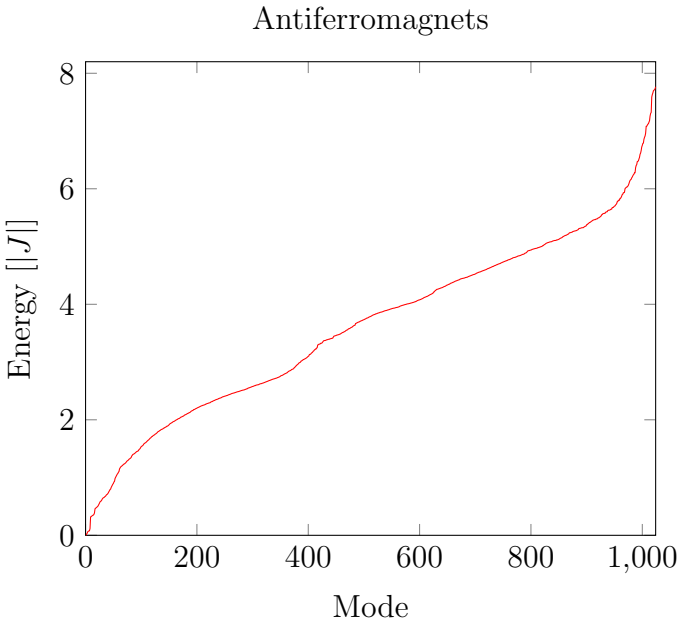

Figure 3.12: Dispersion of the system (antiferromagnets).

3.2.2 Magnon Occupation

Since magnons are bosons, they will obey to the Bose-Einstein statistics (Eq. 2.51). In Fig. 3.13 the average number of magnons in each state is depicted. Different colours correspond to different values of β. As temperature decreases (β increases) less states are occupied, exactly as in ferromagnets

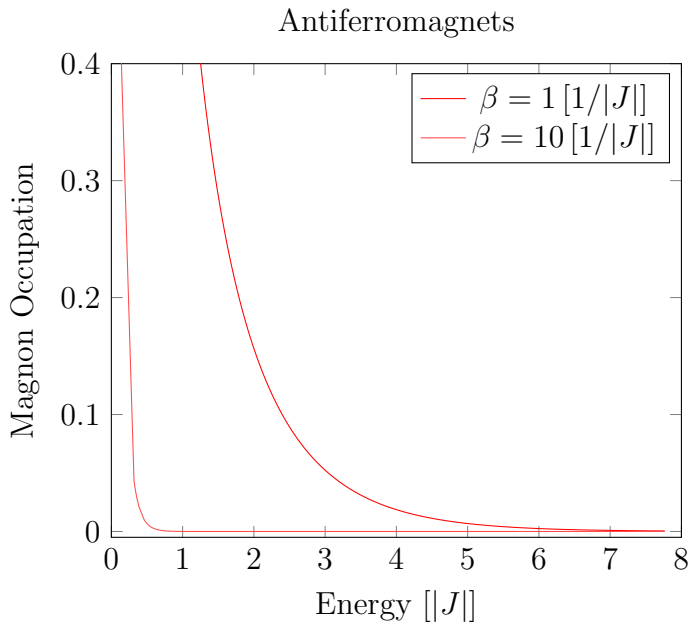

Figure 3.13: Occupation of magnons at each state (antiferromagnets).

3.2.3 Effective Magnetic Field

Unlike the ferromagnetic case, the effective magnetic field distribution of the antiferromagnetic ground state is only computed using the method described in section 2.6.2. The result is shown in Fig. 3.14. Similarly to ferromagnets, the distribution of the effective magnetic field is comparable to the colour plot of the antiferromagnetic ground state, illustrated in Fig. 3.15, which shows that the large numbers of the effective field are due to the skyrmions.

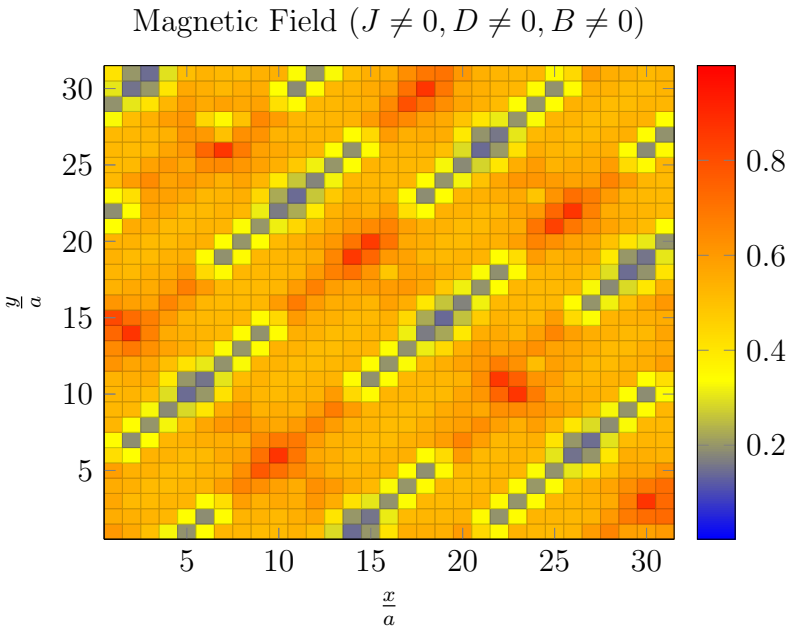

Figure 3.14: Magnetic field distribution using Eq. 2.67 (antiferromagnets).

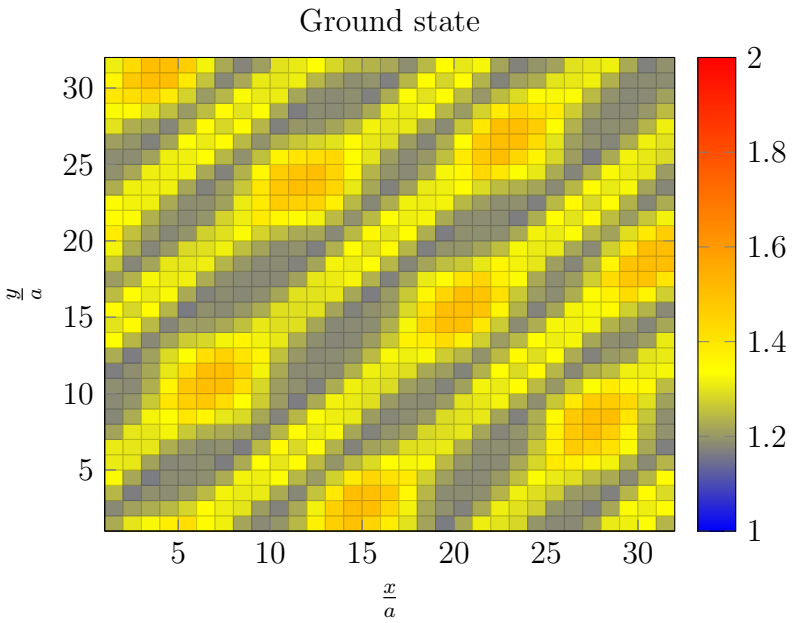

Figure 3.15: Colour plot of the antiferromagnetic ground state.

3.2.4 Comparisons

Similarly to ferromagnets, in this section we compare the results obtained after computing the effective magnetic field using different couplings constants in the Hamiltonian.

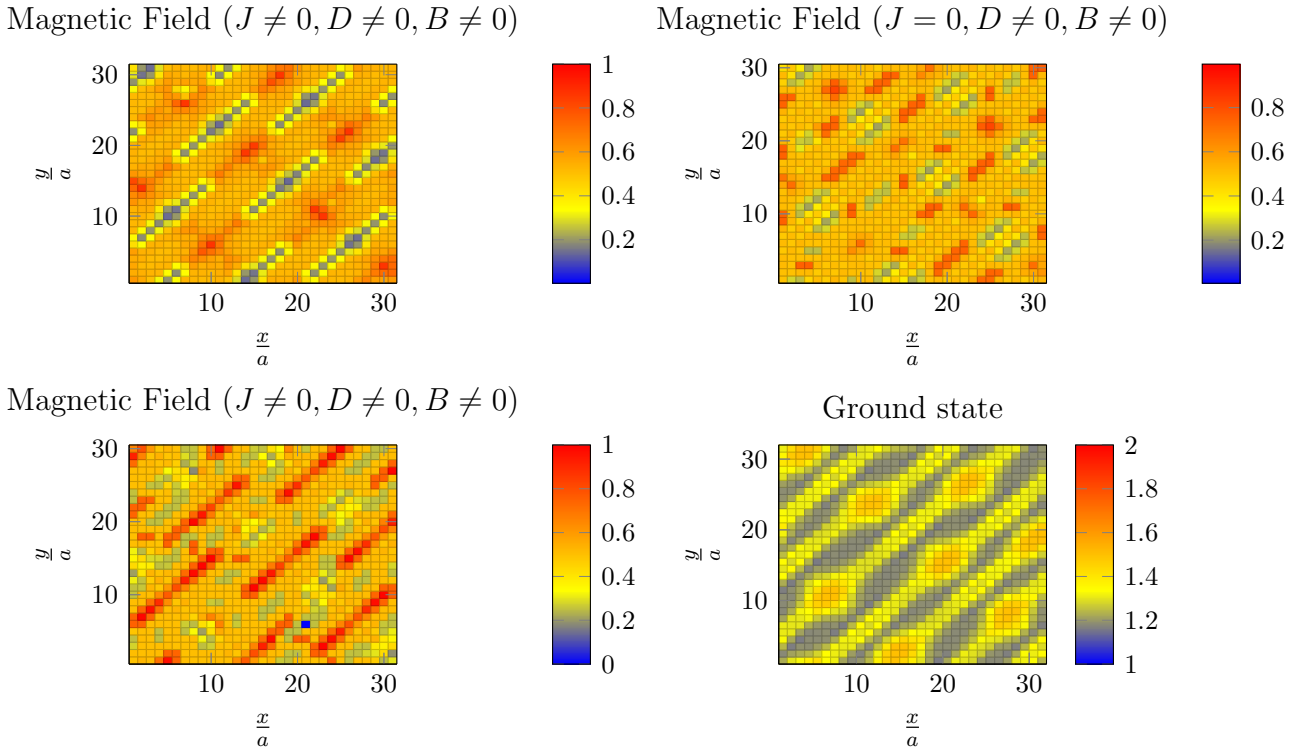

Figure 3.16: Distribution of the effective magnetic field for different values of Hamiltonian's coupling constants (antiferromagnets).

The top left part of Fig. 3.16 is the result already explained in the previous section. The top right part illustrates the distribution of the effective magnetic field if the Hamiltonian had no exchange part and the figure on the bottom left part if the Hamiltonian had no Dzyaloshinskii-Moriya interaction. Finally, the antiferromagnetic ground state is depicted in the bottom right part in order to make the comparison easier. Again, it is visible that the correct result (the one which is similar to the ground state) includes all of the terms in the Hamiltonian, just as in the ferromagnetic case.

3.2.5 Hall Conductivity

Similarly to ferromagnets, we can plot the values of the thermal transverse conductivity as a function of temperature T for antiferromagnets. The important features of Fig. 3.17 are summarised:

- For $T = 0$ there is no conductivity and therefore no Hall effect.
- For $T > 0$, unlike the ferromagnetic case, we can see a non linear behaviour.

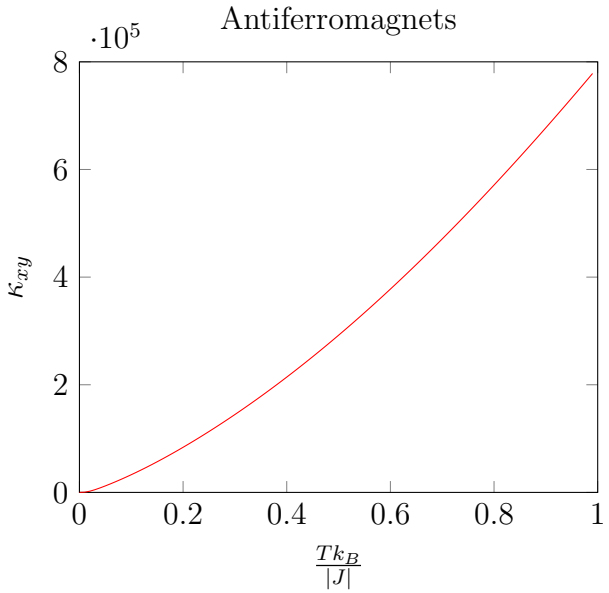

Figure 3.17: Transverse thermal conductivity as a function of temperature in antiferromagnets.

3.3 Comparisons and Conclusion

In this section we compare the results found in the section of ferromagnets with these found in the section of antiferromagnets and give our final conclusion.

Comparing the magnon occupation of ferromagnets with that of the antiferromagnets, we can stress that it does not depend on the character, hence for $\beta = 1$ the two curves are identical as shown in Fig. 3.18. This is expected since the nature is bosonic in both cases.

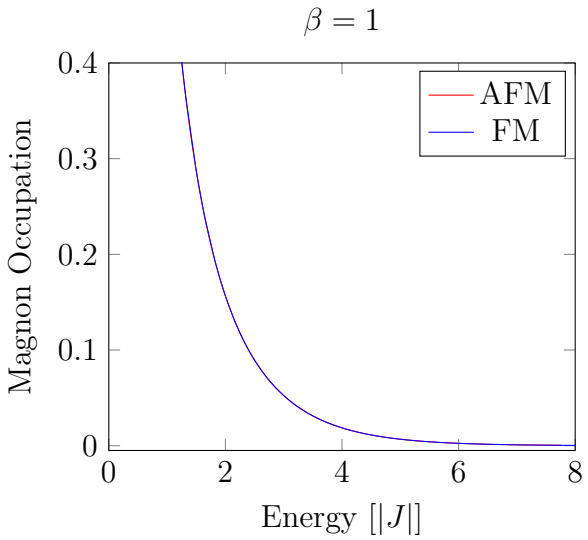

Figure 3.18: Comparison between the occupation number per state in FM and AFM for $\beta = 1$.

Probably the most important figure of the Thesis is the one which illustrates the behaviour of the transverse thermal conductivity for both ferromagnetic and antiferromagnetic configurations in a single diagram. This can be seen in Fig. 3.19 and it allows us to compare the two configurations.

Since the two configurations have to be stable, the freedom of picking a similar one, in both cases is lost. As a consequence, the ground states not only differ in the size but also in the number of skyrmions on them, making the comparison on the same basis almost impossible. This fact prevents us from saying which case is most profitable.

To sum up, by looking at Fig. 3.19 we conclude that the thermal conductivity of the ferromagnetic lattice behaves linearly, whereas the thermal conductivity of the antiferromagnetic lattice has a non-linear behaviour. Furthermore, the antiferromagnetic lattice gives rise to larger absolute values of numbers of conductivities for all values of temperature and therefore it explores a stronger thermal Hall effect. This is not a comparison between the ferromagnetic and the antiferromagnetic case but between

the two given lattices and forms our conclusion.

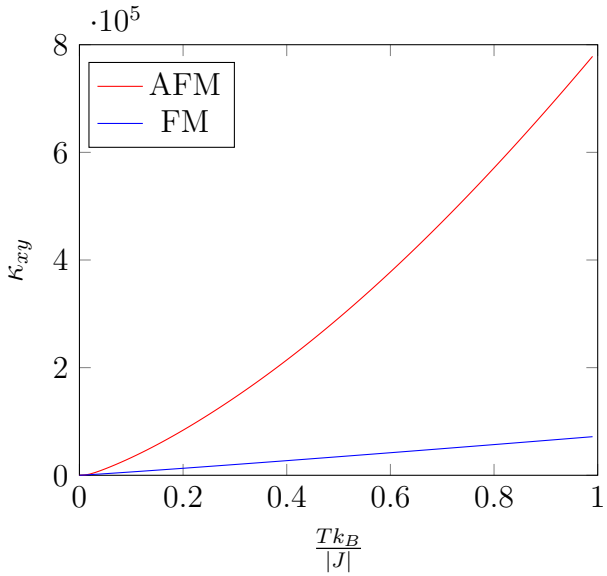

Figure 3.19: Transverse thermal conductivity as a function of temperature in FM and AFM.

CHAPTER 4

Further Research

In this chapter, some suggestions for further research in the specific topic are addressed.

- The transverse thermal conductivity (2.50) is related to some quantities (number of magnons and effective magnetic field) that can be numerically computed as a rule of proportionality instead of a strict mathematical equality. The development of transport theory on numerical basis may directly relate these quantities in a stricter mathematical way.
- The investigation of the thermal Hall effect of magnons is limited to low temperatures where interactions among spin waves and dissipation are negligible phenomena. A complete description of the thermal Hall effect of magnons though requires high-temperature analysis as well, for which the previously mentioned phenomena cannot be neglected.
- Since this topic is experimentally interesting as well, a further suggestion would be to include in the model the coupling of the magnon system to the metallic reservoirs, which is ignored in this Thesis.

Appendices

A

Ferromagnets and Antiferromagnets

As it is known, the quantum number of spin can only take two values for electrons ($s = \frac{1}{2}$ or $s = -\frac{1}{2}$). The former value corresponds to the situation "up", whereas the latter one to the situation "down". Magnetic materials are characterised as "ferromagnets" or "antiferromagnets" depending on the orientation of the spin of their electrons. The left part of Fig. A.2 shows a perfect ferromagnet, in which all spins point to the same direction. In reality there might be some small deviations and still the material to be considered as a ferromagnet. Ferromagnets have a spontaneous magnetisation even in the absence of an external field [21]. In the right part of Fig. A.2 shows a perfect antiferromagnet. The orientation of spin strongly depends on the temperature T. There is a critical temperature T_C, the "Curie temperature", which specifies the magnetic properties of a material. Fig. A.1 summarizes the dependence on the temperature of a magnetic material. It has to be mentioned that the behaviour is similar to both ferromagnets and antiferromagnets.

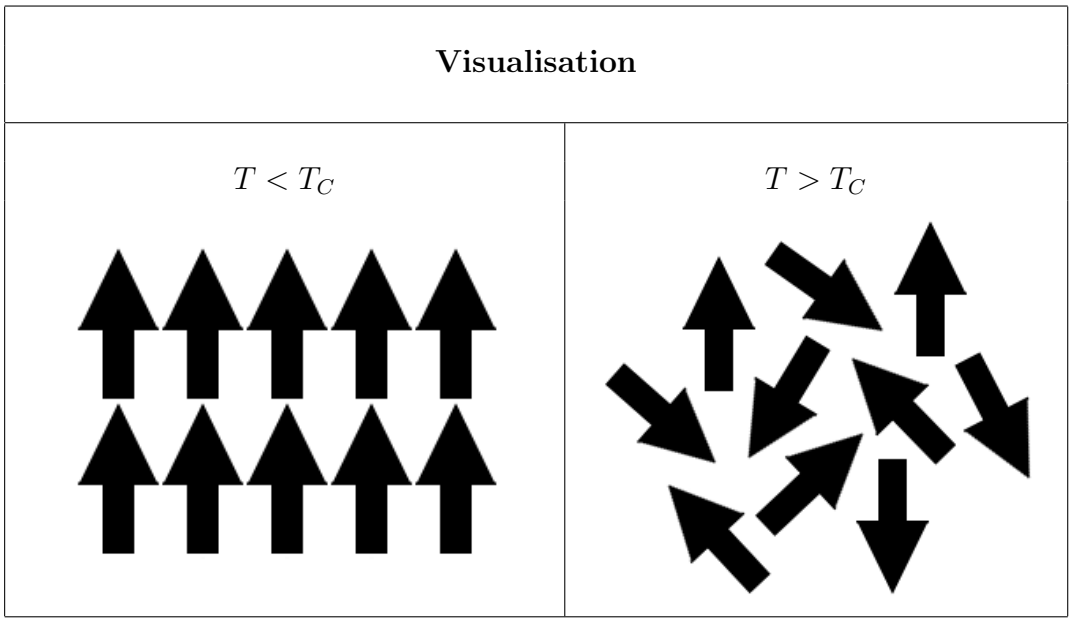

Figure A.1: Temperature dependence of magnetic behaviour.

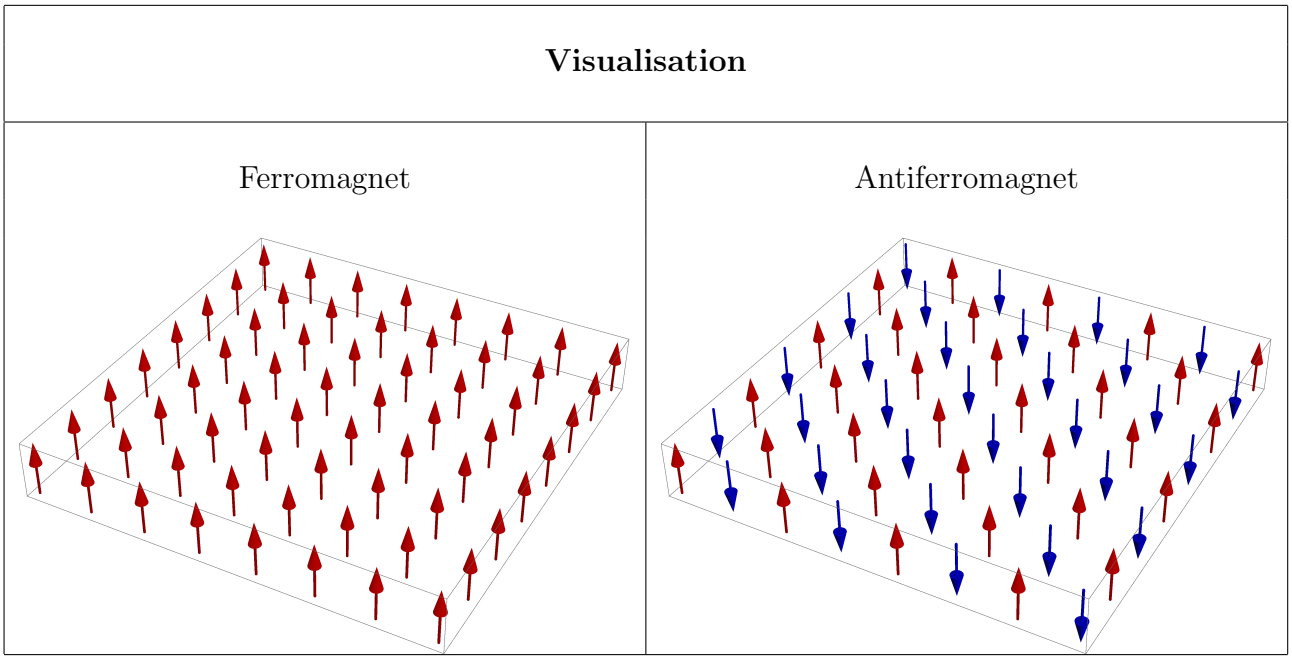

Figure A.2: Ferromagnetic and Antiferromagnetic configurations.

B

Magnon Dispersion Relation

The notion of magnons has already been introduced, however, a complete analysis involves its dispersion relation as well, the derivation of which follows. In this Thesis we are only interested in the behaviour of the dispersion relation and not in the numerical value, hence any constant term will not been taken into account.

The Hamiltonian of a one-dimensional system reads:

$$H = -J \sum_{\langle i,j \rangle} \mathbf{S}_i^A \cdot \mathbf{S}_j^B; \tag{B.1}$$

where A and B correspond to the different sublattices (the one consists of spins pointing up and the other of spins pointing down).

Since only nearest neighbouring interactions are involved, the Hamiltonian B.1 can be written as:

$$H = -\frac{J}{2} \sum_i \mathbf{S}_i^A \cdot \mathbf{S}_{i+1}^B + \mathbf{S}_i^A \cdot \mathbf{S}_{i-1}^B + \mathbf{S}_i^B \cdot \mathbf{S}_{i+1}^A + \mathbf{S}_i^B \cdot \mathbf{S}_{i-1}^A. \tag{B.2}$$

Using that

$$\mathbf{S}_i^A \cdot \mathbf{S}_j^B = S_i^{x,A} S_j^{x,B} + S_i^{y,A} S_j^{y,B} + S_i^{z,A} S_j^{z,B}, \tag{B.3}$$

and that

$$S_x^{A,B} = \frac{S_+^{A,B} + S_-^{A,B}}{2}; \qquad (B.4)$$
$$S_y^{A,B} = \frac{S_+^{A,B} - S_-^{A,B}}{2i},$$

we rewrite the Hamiltonian B.2 as:

$$\begin{aligned} H = -\frac{J}{2}\sum_i \Big[& S_i^{z,A}S_{i+1}^{z,B} + S_i^{z,A}S_{i-1}^{z,B} + S_i^{z,B}S_{i+1}^{z,A} + S_i^{z,B}S_{i-1}^{z,A} \\ & + \frac{1}{2}\left(\mathbf{S}_i^{+,A}\mathbf{S}_{i+1}^{-,B} + \mathbf{S}_i^{-,A}\mathbf{S}_{i+1}^{+,B} + \mathbf{S}_i^{+,A}\mathbf{S}_{i-1}^{-,B} + \mathbf{S}_i^{-,A}\mathbf{S}_{i-1}^{+,B}\right) \\ & + \frac{1}{2}\left(\mathbf{S}_i^{+,B}\mathbf{S}_{i+1}^{-,A} + \mathbf{S}_i^{-,B}\mathbf{S}_{i+1}^{+,A} + \mathbf{S}_i^{+,B}\mathbf{S}_{i-1}^{-,A} + \mathbf{S}_i^{-,B}\mathbf{S}_{i-1}^{+,A}\right)\Big]. \end{aligned} \qquad (B.5)$$

In order to map the spin operators to creation and annihilation operators, we use the Holstein-Primakoff transformations, the first term of the expansion of which are given by:

$$\begin{aligned} S_i^{+,A} &\simeq \sqrt{2S}a_i; \\ S_i^{-,A} &\simeq \sqrt{2S}a_i^\dagger; \\ S_i^{z,A} &\simeq S_i - a_i^\dagger a_i; \\ S_j^{+,B} &\simeq \sqrt{2S}b_j^\dagger; \\ S_j^{-,B} &\simeq \sqrt{2S}b_j; \\ S_j^{z,B} &\simeq S_j - b_j^\dagger b_j. \end{aligned} \qquad (B.6)$$

Plugging Eq. B.6 in Eq. B.5 and neglecting $\mathcal{O}(a^4)$ terms we get:

$$\begin{aligned} H = & \sum_{i\delta} JS\left(a_i b_{i\delta} + a_i^\dagger b_{i+\delta}^\dagger\right) + JS\left(a_i^\dagger a_i^\dagger + b_{i+\delta}^\dagger b_{i+\delta}\right) + \\ & + \sum_{j\delta} JS\left(b_j a_{j+\delta} + b_j^\dagger a_{j+\delta}^\dagger\right) + JS\left(b_j^\dagger b_j + a_{i+\delta}^\dagger a_{i+\delta}\right) + \\ & + C, \end{aligned} \qquad (B.7)$$

with δ to be the number of nearest neighbours (2 for one-dimensional system) and C some unimportant numerical constant.

Hamiltonian B.7 can be further simplified if we transform it in momentum space k. This can be done by defining the following relations.

$$\begin{aligned} a_i &= \frac{1}{\sqrt{N}} \sum_k e^{i\mathbf{k}\cdot\mathbf{x_i}} a_k \\ b_j &= \frac{1}{\sqrt{N}} \sum_k e^{i\mathbf{k}\cdot\mathbf{x_j}} b_k \\ a_i^\dagger &= \frac{1}{\sqrt{N}} \sum_k e^{-i\mathbf{k}\cdot\mathbf{x_i}} a_k^\dagger \\ b_j^\dagger &= \frac{1}{\sqrt{N}} \sum_k e^{-i\mathbf{k}\cdot\mathbf{x_j}} b_k^\dagger \end{aligned} \tag{B.8}$$

Substituting the Fourier transforms of Eq. B.8 in the Hamiltonian B.7 and after some calculations, we get:

$$\begin{aligned} H = &\sum_{k\alpha} JS \cos k\alpha \left(a_k b_{-k} + a_k^\dagger b_{-k}^\dagger \right) + \\ &+ \sum_k JS \left(a_k^\dagger a_k + b_k^\dagger b_k \right) \\ &+ C, \end{aligned} \tag{B.9}$$

with $\alpha_l = x_j - x_i$.

Since Hamiltonian B.9 includes terms with 2 creation (second term) or 2 annihilation (first term) operators, the proper way to diagonilise it is by using the so called Bogoliubov transformations. These transformations introduce some other operators (c_k and d_k) in which the system has to be diagonal. The Bogoliubov relations are defined as:

$$\begin{aligned} c_k &= u_k a_k - v_k b_{-k}^\dagger; \\ d_k &= u_k b_k - v_k a_{-k}^\dagger. \end{aligned} \tag{B.10}$$

Therefore, the inverse transformations are going to be:

$$
\begin{aligned}
a_k &= u_k c_k + v_k d_{-k}^{\dagger};\\
b_k &= u_k d_k + v_k c_{-k}^{\dagger};\\
a_{-k} &= u_k c_{-k} + v_k d_k^{\dagger};\\
b_{-k} &= u_k d_{-k} + v_k c_k^{\dagger};\\
a_k^{\dagger} &= u_k c_k^{\dagger} + v_k d_{-k};\\
b_k^{\dagger} &= u_k d_k^{\dagger} + v_k c_{-k};\\
a_{-k}^{\dagger} &= u_k c_{-k}^{\dagger} + v_k d_k;\\
b_{-k}^{\dagger} &= u_k d_{-k}^{\dagger} + v_k c_k.
\end{aligned}
\tag{B.11}
$$

Hence, the Hamiltonian B.9 becomes:

$$
\begin{aligned}
H = &\sum_{k\alpha} c_k^{\dagger} c_k \left[2JSu_k v_k \gamma_k + JS\left(u_k^2 + v_k^2\right)\right] +\\
&+ \sum_{k\alpha} d_k^{\dagger} d_k \left[2JSu_k v_k \gamma_k + JS\left(u_k^2 + v_k^2\right)\right] +\\
&+ \sum_{k\alpha} \left(c_k d_{-k} + c_k^{\dagger} d_{-k}^{\dagger}\right) \left[JS\gamma_k \left(u_k^2 + v_k^2\right) + 2JSu_k v_k\right] +\\
&+ C,
\end{aligned}
\tag{B.12}
$$

with $\gamma_k = \sum_{\alpha} \cos k\alpha$.

By definition, the coefficients of non diagonal terms (the last two terms in Eq. B.12) have to be zero, hence the following constraint is fulfilled.

$$
\gamma_k \left(u_k^2 + v_k^2\right) + 2u_k v_k = 0. \tag{B.13}
$$

Using that:

$$
\begin{aligned}
u_k &= \cosh \theta_k;\\
v_k &= \sinh \theta_k,
\end{aligned}
\tag{B.14}
$$

we can write Eq. B.13 as:

$$\gamma_k \left(\cosh^2 \theta_k + \sinh^2 \theta_k\right) + 2 \cosh \theta_k \sinh \theta_k = 0. \tag{B.15}$$

However, the following trigonometric relations hold:

$$\begin{aligned} \cosh 2\theta_k &= \cosh^2 \theta_k + \sinh^2 \theta_k; \\ \sinh 2\theta_k &= \cosh \theta_K \sinh \theta_k, \end{aligned} \tag{B.16}$$

therefore, we can write the condition (B.13) as:

$$\gamma_k = -\tanh 2\theta_k. \tag{B.17}$$

Substituting Eq. B.17 in Hamiltonian B.12, we obtain:

$$H = \sum_k \omega_k \left(c_k^\dagger c_k + d_k^\dagger d_k\right) + C, \tag{B.18}$$

with $\omega_k = JSz\sqrt{1-\gamma_k^2}$.

Hamiltonian B.18 is now diagonal. One can see two different types of operators ($c_k/c_k^\dagger$ and $d_k/d_k^\dagger$), each of these annihilate/create a magnon with momentum k and energy ω_k. Hence, each state is degenerate.

Finally, a schematic representation of the ferromagnetic and the antiferromagnetic dispersion of magnons can be seen in Fig. B.1.

B

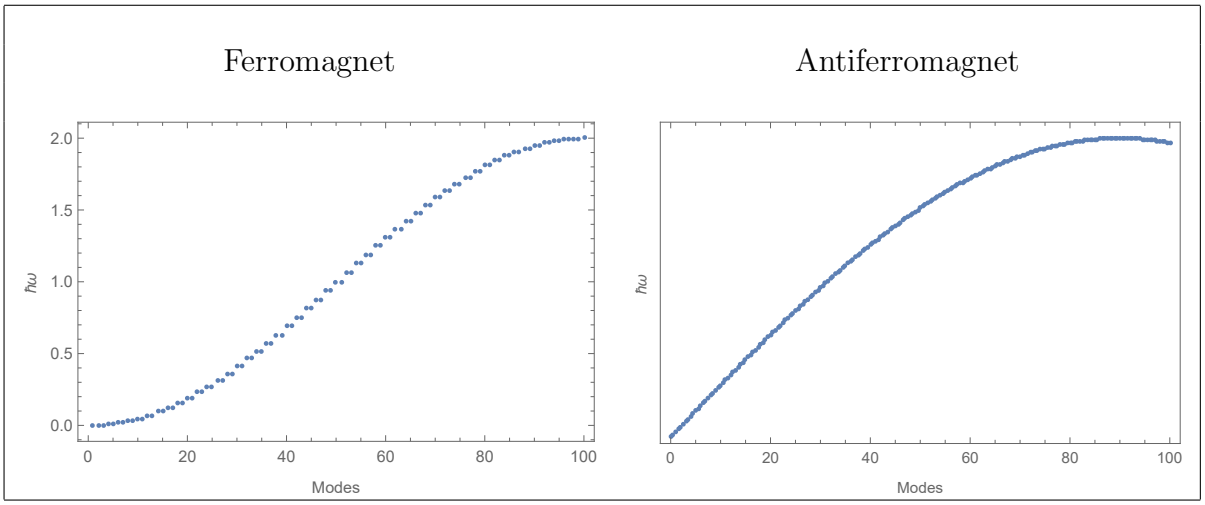

Figure B.1: Ferromagnetic and Antiferromagnetic dispersion.

C

Chirality

Imagine a construction like the one presented in the left part of Fig. C.1, in which different colours stand for different objects. Now imagine that the dashed black line in the middle of the left part of Fig. C.1 represents a mirror. The image that we are going to see is shown in the right part of the figure on the left. As we can see the original construction is identical to the image.

However in nature, there are cases that this is not true. To visualise this reality consider the right part of Fig. C.1. In this case the original construction is not identical to the image and moreover there is no way of making it identical.

The system shown in the right part of Fig. C.1 obeys a property of asymmetry, the so called "Chirality", whereas the system on the left part of Fig. C.1 does not. To sum up, a system is called "chiral" if and only if it is distinguishable from its mirror image.

4

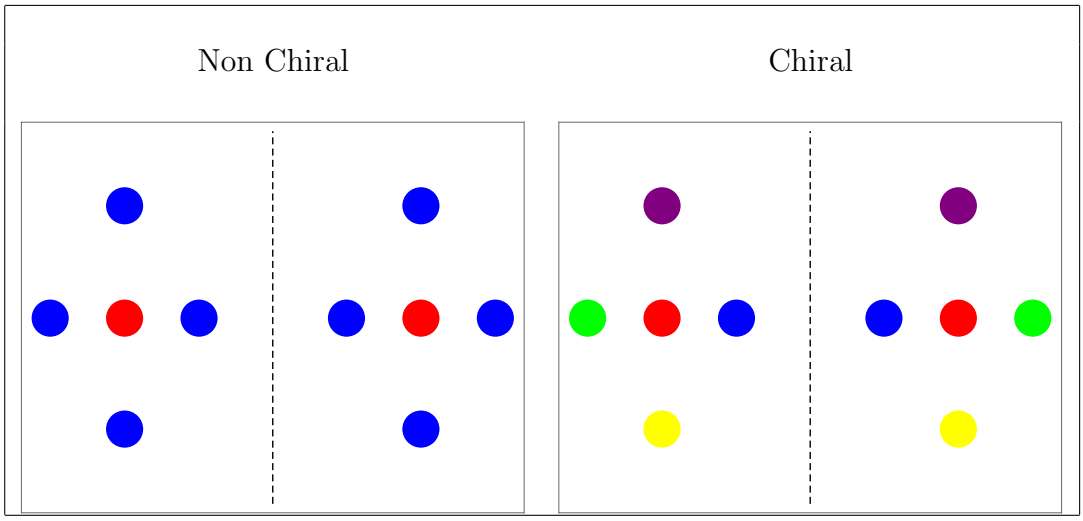

Figure C.1: Chiral and non Chiral system.

References

[1] Y. Onose, T. Ideue, H. Katsura, Y. Shiomi, N. Nagaosa, and Y. Tokura, "Observation of the Magnon Hall Effect," *Science*, vol. 329, no. 5989, pp. 297–299, 2010.

[2] S. Mühlbauer, B. Binz, F. Jonietz, C. Pfleiderer, A. Rosch, A. Neubauer, R. Georgii, and P. Böni, "Skyrmion lattice in a chiral magnet," *Science*, vol. 323, no. 5916, pp. 915–919, 2009.

[3] R. Keesman, M. Raaijmakers, A. Baerends, G. Barkema, and R. Duine, "Skyrmions in square-lattice Antiferromagnets," *arXiv preprint arXiv:1603.03688*, 2016.

[4] "What are magnons?." `https://www.uni-muenster.de/Physik.AP/Demokritov/en/Forschen/Forschungsschwerpunkte/mBECwam.html`. Accessed: 2010-08-30.

[5] K. A. van Hoogdalem, Y. Tserkovnyak, and D. Loss, "Magnetic texture-induced thermal hall effects," *Phys. Rev. B*, vol. 87, p. 024402, Jan 2013.

[6] "Timezones." `http://militarytimechart.com/time-zones-explained/`. Accessed: 2010-09-30.

[7] K. Everschor-Sitte and M. Sitte, "Real-space berry phases: Skyrmion soccer," *Journal of Applied Physics*, vol. 115, no. 17, p. 172602, 2014.

[8] D. J. Griffiths and E. G. Harris, "Introduction to quantum mechanics," *American Journal of Physics*, vol. 63, no. 8, pp. 767–768, 1995.

[9] M. I. Kaganov, *Electrons, Photons, Magnons*. Mir Publishers Moscow, 1981.

[10] M. G. Cottam, *Linear and Nonlinear Spin Waves in Magnetic Films and Superlattices*. World Scientific Publishing, 1994.

[11] S. A. Owerre, "Magnon hall effect in ab-stacked bilayer honeycomb quantum magnets," *Phys. Rev. B*, vol. 94, p. 094405, Sep 2016.

[12] R. Resta, "Manifestations of Berry's Phase in Molecules and Condensed Matter," *Journal of Physics: Condensed Matter*, vol. 12, pp. R107+, Mar. 2000.

[13] G. Yin, Y. Li, L. Kong, R. K. Lake, C. L. Chien, and J. Zang, "Topological charge analysis of ultrafast single skyrmion creation," *Phys. Rev. B*, vol. 93, p. 174403, May 2016.

[14] M. Menzel, *Non-collinear magnetic ground states observed in iron nanostructures on iridium surfaces*. Verlag Dr. Hut, 2011.

[15] K. Uchida, J. Xiao, H. Adachi, J.-i. Ohe, S. Takahashi, J. Ieda, T. Ota, Y. Kajiwara, H. Umezawa, H. Kawai, *et al.*, "Spin seebeck insulator," *Nature materials*, vol. 9, no. 11, pp. 894–897, 2010.

[16] Y. Kajiwara, K. Harii, S. Takahashi, J. Ohe, K. Uchida, M. Mizuguchi, H. Umezawa, H. Kawai, K. Ando, K. Takanashi, *et al.*, "Transmission of electrical signals by spin-wave interconversion in a magnetic insulator," *Nature*, vol. 464, no. 7286, pp. 262–266, 2010.

[17] F. Meier and D. Loss, "Magnetization transport and quantized spin conductance," *Phys. Rev. Lett.*, vol. 90, p. 167204, Apr 2003.

[18] J. Barker and O. A. Tretiakov, "Static and dynamical properties of antiferromagnetic skyrmions in the presence of applied current and temperature," *Physical review letters*, vol. 116, no. 14, p. 147203, 2016.

[19] B. Zimmermann, *Calculation of the Dzyaloshinskii-Moriya Interaction in ultrathin magnetic Films: Cr/W (110)*. PhD thesis, Diploma thesis, RWTH Aachen, 2010.

[20] G. Butenko, "Phenomenological theory of chiral states in magnets with dzyaloshinskii-moriya interactions," 2012.

[21] S. Blundell, *Magnetism in Condensed Matter (Oxford Master Series in Physics)*. Oxford University Press, USA, 1 ed., Dec. 2001.

[22] M. Bode, M. Heide, K. von Bergmann, P. Ferriani, S. Heinze, G. Bihlmayer, A. Kubetzka, O. Pietzsch, S. Blügel, and R. Wiesendanger, "Chiral magnetic order at surfaces driven by inversion asymmetry," *Nature*, vol. 447, no. 7141, pp. 190–193.

[23] B. van Dijk, "Skyrmions and the dzyaloshinskii-moriya interaction," 2015.

[24] R. Keesman, A. O. Leonov, P. van Dieten, S. Buhrandt, G. T. Barkema, L. Fritz, and R. A. Duine, "Degeneracies and fluctuations of néel skyrmions in confined geometries," *Phys. Rev. B*, vol. 92, p. 134405, Oct 2015.

[25] A. Roldán-Molina, M. Santander, A. Núnez, and J. Fernández-Rossier, "Quantum Theory of Spin Waves in Finite Chiral Spin Chains," *Physical Review B*, vol. 89, no. 5, p. 054403, 2014.

[26] J. T. Haraldsen and R. S. Fishman, "Spin Rotation Technique for non-collinear Magnetic Systems: Application to the Generalized Villain Model," *Journal of Physics: Condensed Matter*, vol. 21, no. 21, p. 216001, 2009.

[27] A. Roldán-Molina, M. Santander, A. Nunez, and J. Fernández-Rossier, "Quantum Fluctuations Stabilize Skyrmion Textures," *Physical Review B*, vol. 92, no. 24, p. 245436, 2015.

[28] M.-w. Xiao, "Theory of Transformation for the Diagonalization of Quadratic Hamiltonians," *arXiv preprint arXiv:0908.0787*, 2009.

[29] J. Van Hemmen, "A Note on the Diagonalization of Quadratic Boson and Fermion Hamiltonians," *Zeitschrift für Physik B Condensed Matter*, vol. 38, no. 3, pp. 271–277, 1980.

[30] J. Colpa, "Diagonalization of the quadratic boson hamiltonian," *Physica A: Statistical and Theoretical Physics*, vol. 93, pp. 327–353, Sept. 1978.

[31] R. Matsumoto and S. Murakami, "Theoretical prediction of a rotating magnon wave packet in ferromagnets," *Phys. Rev. Lett.*, vol. 106, p. 197202, May 2011.

[32] V. K. Dugaev, P. Bruno, B. Canals, and C. Lacroix, "Berry phase of magnons in textured ferromagnets," *Phys. Rev. B*, vol. 72, p. 024456, Jul 2005.

[33] M. Aidelsburger, *Artificial gauge fields with ultracold atoms in optical lattices*. Springer, 2016.

[34] H. Katsura, N. Nagaosa, and P. A. Lee, "Theory of the thermal hall effect in quantum magnets," *Physical review letters*, vol. 104, no. 6, p. 066403, 2010.

[35] J. Ibañez-Azpiroz, A. Eiguren, A. Bergara, G. Pettini, and M. Modugno, "Breakdown of the peierls substitution for the haldane model with ultracold atoms," *Physical Review A*, vol. 90, no. 3, p. 033609, 2014.

[36] D. Sen and R. Chitra, "Large- U limit of a hubbard model in a magnetic field: Chiral spin interactions and paramagnetism," *Phys. Rev. B*, vol. 51, pp. 1922–1925, Jan 1995.

[37] P. Bruno, V. Dugaev, and M. Taillefumier, "Topological hall effect and berry phase in magnetic nanostructures," *Physical review letters*, vol. 93, no. 9, p. 096806, 2004.

[38] T. Schulz, R. Ritz, A. Bauer, M. Halder, M. Wagner, C. Franz, C. Pfleiderer, K. Everschor, M. Garst, and A. Rosch, "Emergent electrodynamics of skyrmions in a chiral magnet," *Nature Physics*, vol. 8, no. 4, pp. 301–304, 2012.

[39] A. Neubauer, C. Pfleiderer, B. Binz, A. Rosch, R. Ritz, P. Niklowitz, and P. Böni, "Topological hall effect in the a phase of mnsi," *Physical review letters*, vol. 102, no. 18, p. 186602, 2009.

[40] W. Research, "Mathematica 10.1," 2015.

[41] C. Sanderson, "Armadillo: An Open Source C++ Linear Algebra Library for Fast Prototyping and Computationally Intensive Experiments," tech. rep., NICTA, Sept. 2010.